Title

Single-cell profiling of Arabidopsis leaves to Pseudomonas syringae infection

Journal

Cell Reports, 42(7)

ISSN

2639-1856

Authors

Zhu, Jie

Lolle, Signe

Tang, Andrea

et al.

Publication Date

2023-07-01

DOI

10.1016/j.celrep.2023.112676

Peer reviewed

Published in final edited form as:

Cell Rep. 2023 July 25; 42(7): 112676. doi:10.1016/j.celrep.2023.112676.

Single-cell profiling of *Arabidopsis* leaves to *Pseudomonas syringae* infection

Jie Zhu[1], **Signe Lolle**[1], **Andrea Tang**[1], **Bella Guel**[1], **Brian Kvitko**[2], **Benjamin Cole**[3,*], **Gitta Coaker**[1,4,*]

[1]Department of Plant Pathology, University of California, Davis, Davis, CA 95616, USA

[2]Department of Plant Pathology, University of Georgia, Athens, GA 30602, USA

[3]DOE Joint Genome Institute, Lawrence Berkeley National Laboratory, Berkeley, CA 94720, USA

[4]Lead contact

SUMMARY

Plant response to pathogen infection varies within a leaf, yet this heterogeneity is not well resolved. We expose *Arabidopsis* to *Pseudomonas syringae* or mock treatment and profile >11,000 individual cells using single-cell RNA sequencing. Integrative analysis of cell populations from both treatments identifies distinct pathogen-responsive cell clusters exhibiting transcriptional responses ranging from immunity to susceptibility. Pseudotime analyses through pathogen infection reveals a continuum of disease progression from an immune to a susceptible state. Confocal imaging of promoter-reporter lines for transcripts enriched in immune cell clusters shows expression surrounding substomatal cavities colonized or in close proximity to bacterial colonies, suggesting that cells within immune clusters represent sites of early pathogen invasion. Susceptibility clusters exhibit more general localization and are highly induced at later stages of infection. Overall, our work shows cellular heterogeneity within an infected leaf and provides insight into plant differential response to infection at a single-cell level.

Graphical Abstract

[*]Correspondence: bjcole@lbl.gov (B.C.), glcoaker@ucdavis.edu (G.C.).

AUTHOR CONTRIBUTIONS

Conceptualization, J.Z., S.L., B.C., and G.C.; Investigation, J.Z., S.L., B.C., A. T., B.K., and B.G.; Writing – Original Draft, J.Z., B.C., and G.C.; Writing – Review & Editing, J.Z. and G.C.; Supervision, G.C.; Funding Acquisition, G.C.

SUPPLEMENTAL INFORMATION

Supplemental information can be found online at https://doi.org/10.1016/j.celrep.2023.112676.

DECLARATION OF INTERESTS

The authors declare no competing interests.

INCLUSION AND DIVERSITY

We support inclusive, diverse, and equitable conduct of research.

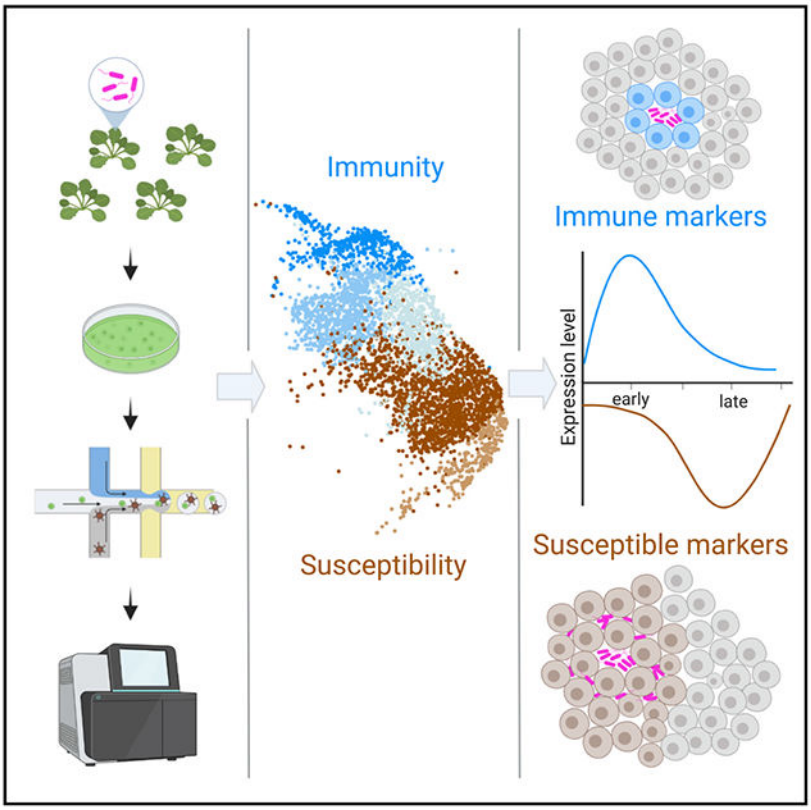

In brief

Zhu et al. report the plant response to *Pseudomonas* infection at single-cell resolution, showing that leaves exhibit cell populations at opposing states (immune and susceptible). Immune and susceptible cell populations are determined by bacterial colony size and infection time. Their study provides a framework for high-resolution exploration of plant host-pathogen interactions.

INTRODUCTION

Plants can be infected by diverse pathogens capable of colonizing roots, vascular tissues, and foliar (leaf) tissue. Many plant diseases exhibit variable symptoms. For example, inoculation of bacteria or fungal spores using infiltration or spray results in unequal symptom development and a relatively small proportion of pathogens successfully invade their hosts.[1–3] Moreover, different stages of pathogen infection are often observed within a leaf.[4,5] Heterogeneity in pathogen distribution and, likely, the plant response affects symptom development.[6] Strains of the bacterial pathogen *Pseudomonas syringae* have a broad host range and can infect many economically important plant species, causing a variety of foliar symptoms.[7,8]

Mechanisms regulating pathogen distribution and colonization on plants can be a combination of physical, metabolic, and immune barriers. Physical barriers, such as trichomes, the waxy cuticle, plant cell walls, and closed stomatal pores can regulate the penetration of pathogens into the plant interior.[9,10] Plants can also recognize pathogen

molecular features, including damage and effectors, using either surface-localized or intracellular immune receptors.[11] Surface-localized pattern recognition receptors (PRRs) detect microbe-associated molecular patterns (MAMPs) or damage-associated molecular patterns (DAMPs), resulting in PRR-triggered immunity (PTI). Immune recognition leads to a series of downstream defense responses, including calcium influx, the production of reactive oxygen species, defense hormone production, and global transcriptional reprogramming.[12,13] PTI can be generally induced against diverse pathogens because of the conserved nature of MAMPs (e.g., bacterial flagellin and elongation factor Tu, fungal chitin).[13] However, virulent pathogens secrete metabolites and proteinaceous effectors that dampen immunity and establish suitable environments for growth.[14] Thus, plant-pathogen interactions are a highly dynamic process, resulting in heterogeneous cellular responses.

Past studies investigating plant-pathogen interactions mainly depend on assays from bulk tissue (i.e., whole leaf or roots). Although genome-wide transcriptional profiling has advanced our understanding of immune responses, cellular responses are averaged across entire tissues.[15,16] Single-cell RNA sequencing (scRNA-seq) technologies enable massively parallel transcriptional profiling of thousands of cells.[17–20] scRNA-seq interrogates populations at the single-cell level and on a genome-wide scale to profile transcriptomes from different cell types and cell states.[18,21] The application of scRNA-seq in plants has provided new insight into cell identity, function, and development in different tissues.[22–27] With respect to pathogen infection, it remains unclear how large populations of plant cells within a tissue respond and how pathogen proximity influences cellular responses at high resolution.

In this study, we combined scRNA-seq and live-cell imaging of fluorescent reporters to investigate plant cellular responses to pathogen infection. We established a transcriptome atlas of *Arabidopsis* leaf tissue infected with virulent *P. syringae*. The atlas enabled the identification of pathogen-responsive cell clusters at immune, transition, and susceptible states. Pseudotime trajectory revealed a continuum of disease progression from an immune to a susceptible state. We validated this trajectory using fluorescent transcriptional reporter lines expressing either immune or susceptible cell cluster markers identified by scRNA-seq. Finally, we identified diverse spatial and temporal patterns of immune and susceptible marker genes that can be influenced by pathogen proximity.

RESULTS

scRNA-seq profiling of *Arabidopsis* leaf tissue infected with *P. syringae*

To investigate plant responses to pathogen infection at high resolution, we first analyzed bacterial distribution within a leaf. We compared the bacterial distribution between wild-type *P. syringae* pv. tomato DC3000 3xmCherry with the DC3000 *ΔhopQ1* 3xmCherry at 0, 4, 10, and 24 h post-inoculation (hpi; Figure S1). Both bacterial strains behaved identically. The *hopQ1* effector deletion strain, frequently used as a tool to investigate *P. syringae*, is fully virulent on *Arabidopsis* and also infects *Nicotiana benthamiana*.[28] Therefore, we used virulent *P. syringae* pv. tomato DC3000 *ΔhopQ1* labeled with 3xmCherry (hereafter *Pst* DC3000) for our experiments. *Pst* DC3000 was inoculated on four-week-old *Arabidopsis thaliana*. We observed patchy distribution of *Pst* DC3000 as well as differences in colony

number and area within a leaf at 24 hpi, suggesting that bacterial colonization is spatially variable (Figures 1A–1C). At this infection stage, *Arabidopsis* leaves do not exhibit visible symptoms, but bacteria multiply aggressively.[7,29]

Pst DC3000 colonizes the intercellular space between mesophyll cells, manipulating them to provide more favorable conditions for microbial growth. To characterize the dynamics of the interaction between *Pst* DC3000 and *Arabidopsis* mesophyll tissue, we enriched for mesophyll cells using the Tape-*Arabidopsis* Sandwich method (Figure 1D).[30] Single-cell transcriptomes were then profiled from *Pst* DC3000- and mock-treated samples 24 hpi using the 10X Genomics scRNA-seq platform (Figure 1D). We recovered 11,895 single-cell transcriptomes with a median number of 3,521 genes and 17,017 unique transcripts, representing more than 80% of protein-coding genes in the *Arabidopsis* genome (Figures S2A and S2B). Complementing our single-cell datasets, we also performed bulk RNA sequencing (RNA-seq) for protoplasts and infiltrated leaves to identify genes modulated in response to pathogen infection ($n = 890$, adjusted $p < 0.01$, log fold-change > 2), as well as genes possibly affected by protoplast generation ($n = 7,548$, adjusted $p < 0.01$, log fold-change > 0.5; Table S1A). There was a strong correlation between merged single-cell and bulk protoplasts samples (Spearman's rho = 0.786 and 0.848 for mock- and bacteria-treated samples, respectively; Figure S2C), indicating that protoplasting did not severely affect most genes' expression. We excluded protoplast-inducible genes from further analysis of our single-cell dataset.

Using graph-based unsupervised clustering, we identified 18 major cell clusters and visualized them on a uniform manifold approximation and projection (UMAP) plot (Figure 1E). Each cluster contained cells from both *Pst* DC3000- and mock-treated leaves (Figures 1E and S2D). To assign cell types, we used a recently published single-cell transcriptomics survey of *Arabidopsis* leaf tissue,[23] as well as expression of well-known cell type markers. The predominant predicted identity of cells within each cluster was then used to assign a cell type to the whole cluster. We also integrated our single-cell datasets with five previously published *Arabidopsis* leaf scRNA-seq datasets.[23–25,31,32] Analysis of the integrated dataset suggests that the vast majority of cells profiled in this study are similar in cell type as those profiled by others, with the exception of an increased density of *Pst* DC3000-treated cells within the larger mesophyll cell cluster (Figures S2F–S2N). The 18 cell clusters contain eight cell types, but exhibit predominant mesophyll identity (~93.7% of all cells, clusters M1–M14; Figures 1E, 1F, and S2D).

scRNA-seq reveals cell clusters ranging from immunity to susceptibility within a leaf

Integrative analysis of cells from *Pst* DC3000- and mock-treatment revealed a large subpopulation of cells from infected leaves constituting clusters M1–M5 (Figures S2D, S3A, and S3B). More than 70% of cells in clusters M1–M5 were exposed to pathogen treatment, representing 34.8% of all cells. Further examination revealed that expression of genes induced by bacterial infection in these five clusters were generally higher than other clusters (Figure S3C). We refer to these five clusters, M1–M5, as pathogen-responsive clusters. Some of the cells in pathogen-responsive clusters were from the mock-treated sample (Figures S2D, S3A, and S3B). We then re-clustered cells from mock-treated

sample and examined the distribution of cell populations defined from the integrated dataset. Cells in clusters M1–M5 still remained their unique character, although they were more diffuse than when combined with DC3000-treated cells (Figure S4A). The plants used for this study were grown on soil (not in axenic conditions) and we hypothesize soil-borne or environmental bacteria that might elicit a defense response from the plant as previously described.[33] We examined whether impacts from protoplasting could have resulted in segmentation of this cell population. Here, we derived a protoplast signature score representing scaled expression across the set of genes found to be induced by protoplasting (Figure S2E). Although some cell clusters exhibited relatively high protoplast-related expression, this could not completely explain the separation of cells from treated and untreated populations (Figure S2E). Taken together, our results indicate major differential shifts in the plant cell response after pathogen exposure.

To investigate the transcriptional reprogramming occurring in each pathogen-responsive cluster, we carried out Gene Ontology (GO) analyses. Clusters M1 and M2 exhibited enrichment of GO terms related to defense response to bacterium, immune response, and response to salicylic acid (SA) (Figure S3D). Clusters M4 and M5 were enriched in terms related to response to jasmonic acid (JA) and water transport (Figure S3D). These results suggest opposite transcriptional responses in clusters M1 and M2 versus clusters M4 and M5. To confirm this result, we calculated immune and susceptibility response scores based on gene expression modules for sets of genes known to be involved in immunity or disease and were differentially expressed in our bulk RNA-seq analysis (Figure 2A; Table S1B). Consistent with the GO analyses, clusters M1 and M2 displayed a higher immune response score, while M4 and M5 displayed a higher susceptibility response score (Figure 2A). Cluster M3 did not display a strong average response score (Figure 2A).

Next, we analyzed the expression of known genes involved in immunity and susceptibility to *Pst* DC3000 (Figure 2B). Expression of known plant immune-related genes *CALMODULIN BINDING PROTEIN 60g (CBP60g), ENHANCED DISEASE SUSCEPTIBILITY 5 (EDS5), FLG22-INDUCED RECEPTOR-LIKE KINASE 1 (FRK1)* and *PATHOGENESIS-RELATED 1 (PR1)* was induced in clusters M1 and M2 compared with non-responsive mesophyll cell clusters (M6–M14). In contrast, clusters M4 and M5 displayed induced expression of genes in susceptibility including those responded to JA and abscisic acid (ABA) (e.g., *CHLOROPHYLLASE 1/CORONATINE INDUCED 1 [CORI1], CORONATINE INDUCED 3 [CORI3]*, and *ABA INSENSITIVE 1* [*ABI1*]). *Pst* DC3000 induces JA signaling through production of coronatine, but protoplasting can also induce JA.[34–36] Although pathogen-responsive clusters had low protoplast signature scores, other clusters with JA GO term induction had higher protoplast induced scores, which may be the result of incomplete gene removal (Figures S2E and S3D). Specific transcripts related to both immunity and susceptibility were induced in cluster M3, but at lower magnitude compared with clusters M1–M2 and clusters M4–M5, suggesting a transition state between immunity and susceptibility (Figures 2A and S4B). Cluster M2 exhibited the strongest activation of immune-related genes and related biological processes (Figures 2A, 2B, and S3D). These data indicate that M1 and M2 represent immune-activated clusters, M3 is a transition cluster, and M4 and M5 represent susceptibility clusters (Figures 2A and 2B).

Pst DC3000 is able to cause disease on *Arabidopsis* and consistent with a compatible interaction, M5 represents the largest cluster (14.2% of 11,895 cells; Figure S2D).

Within a tissue, there are multiple points of infection representing different stages of disease development. Pseudotime analyses, which aim to order cells relative to a temporal, developmental, or treatment axis, have been used to model the trajectory of a biological process, with each cell signifying a singular time point along a continuum.[37] In order to predict the trajectory of pathogen-responsive cellular clusters, we performed pseudotime analysis using Monocle 3.[37–40] To circumvent influence of different cell types, we used *Pst* DC3000-treated mesophyll cells from clusters M1–M14 to infer the trajectory of disease progression. The trajectory was mostly linear, progressing through nonpathogen-responsive clusters (M6–M14), followed by immune clusters (M1 and M2), the transition cluster M3 and ended in the susceptible clusters (M4 and M5; Figure 2C). In order to investigate pathogen responsiveness through pseudotime, a signature score was computed to quantify the overall impact *Pst* DC3000 has on each cell using module scores from genes identified as differentially expressed in our bulk RNA-seq data. When overlaid upon pseudotime, the *Pst* DC3000 signature score was markedly induced in cells undergoing immunity (clusters M1 and M2), then plateaued or decreased through cells experiencing features associated with disease susceptibility (clusters M3–M5), consistent with the dynamic nature of plant-pathogen interactions (Figure 2D). These results indicate in a compatible interaction, disease progresses from plant defense, into a transitional state and culminates in susceptibility.

We also sought to identify genes that have dynamic expression patterns relative to the imputed pseudotime axis. Here, we again used Monocle 3 to identify genes that vary significantly with pseudotime, retrieving 776 loci (Figure S5; Table S1C). We clustered these into seven groups, with two clusters having expression profiles consistent with a susceptibility response (clusters 2 and 6), while four clusters had profiles consistent with immunity or the transition between immunity and susceptibility (clusters 3–5 and 7) (Figure S5; Table S1C). Genes within clusters consistent with a susceptibility or immune response represent candidates important in disease progression (Figure S5). We also identified unique transcripts expressed in immunity, transition, and susceptibility clusters (Figure S4B).

Visualization of immune and susceptible cellular markers during disease progression

We sought to experimentally validate pseudotime predictions and investigate expression of immune and susceptible markers through the course of infection. We used surface inoculation, which more closely mimics natural infection, on two-week-old *Arabidopsis* seedlings. This protocol also allows inoculation of younger plants to facilitate imaging by confocal microscopy. In order to test the experimental setup, we first monitored the growth of *Pst* DC3000-mCherry (Figure 3A). Bacterial titers did not change in the first 4 hpi, but dramatically increased from 24 to 72 hpi, consistent with previous experiments on seedlings and soil-grown plants (Figure 3A, left).[7,41] We visualized spatio-temporal dynamics of bacterial colonization after surface inoculation. At 24 hpi, spotty fluorescence signals were observed (Figure 3A, middle), which was similar to syringe infiltration (Figure 1A). Visualizing multiple focal planes of bacterial fluorescence signals demonstrated that bacteria colonized intercellular space between mesophyll cells by 24 hpi. At 48 and 72

hpi, we observed enlarged and merged fluorescent spots, indicating high multiplication of bacterial populations at these stages (Figure 3A, middle). Quantification of fluorescence intensity per colony showed a continuous increase over time (Figure 3A, right).

We then visualized the expression patterns of cell cluster marker genes and fluorescently tagged *Pst* DC3000 during the course of infection. We selected marker genes that showed relatively high and specific expression from scRNA-seq analyses in either immune or susceptible clusters. Fluorescent transcriptional reporter lines coupled to a nuclear localization signal (NLS) enabled visualization of cell-specific plant responses during pathogen infection.

Three immune marker genes were selected: *FRK1*, *AT3G18250* (*LIPOPROTEIN 1, LipoP1*), and *CBP60g*. *FRK1* is a receptor-like kinase that is strongly induced during pattern-triggered immunity and at early stages after pathogen infection.[42,43] *LipoP1* is a putative membrane lipoprotein, whose function is unknown. The *CBP60g* transcription factor regulates biosynthesis of the plant defense hormone SA.[44,45] All three markers displayed high expression in immune clusters M1 and M2, variable expression in the transition cluster M3, but low expression in susceptible clusters M4 and M5 (Figures 3B–3D left, Figure S7A).

Using a previously characterized transcriptional reporter *pFRK1::NLS-3xmVENUS*[46] and newly generated transgenic lines *pLipoP1/pCBP60g::NLS-3xmCitrine*, we observed low fluorescence signals in mock-inoculated *Arabidopsis* true leaves (Mock, Figures 3B–3D). A time course experiment was able to detect *FRK1* expression at earlier time points (4 and 10 h), but the induction was weaker and not significant from the mock inoculation (Figure S6A). *FRK1* expression was strongly induced at 24 hpi and dramatically downregulated at 48 and 72 hpi (Figure 3B). *FRK1* was previously shown to be strongly induced 2 h post-syringe infiltration with *Pst* DC3000 using qPCR.[43] These results suggest that the expression of *FRK1* at 24 hpi represents an early infection stage using surface inoculation. We observed the expression of *LipoP1* and *CBP60g* was highly induced at 24–48 hpi (Figures 3C and 3D). All three immune markers *FRK1*, *CBP60g*, and *LipoP1* exhibited more localized induction at 24 hpi. The expression of all immune markers was significantly reduced at 72 hpi when plants exhibited chlorosis and water-soaked symptoms (Figures 3B–3D). A second independent transgenic line of *pLipoP1::NLS-3xmCitrine* exhibited a similar expression pattern, but had more robust expression at 72 h (Figure S6C). Compared with *CBP60g* and *FRK1, LipoP1* exhibited stronger expression in the transition cluster M3, which might result in stochasticity of the late expression of this gene in different lines (Figures 3C and S6C). We screened four transcriptional reporter lines of *CBP60g* (Figure S7F). Three of them (22-1, 22-18, and 22-23) had similar pattern of expression and exhibited localized expression surrounding bacterial colonies at 24 hpi. In contrast, one *CBP60g* line (22-4) was induced at 24 h but did not exhibit localized expression (Figure S7F). Together, these data highlight activation of immune marker genes at early infection stages and downregulation at late stages, consistent with the pseudotime trajectory.

We explored expression of three susceptibility marker genes strongly expressed in clusters M4 and M5: *EXPANSIN 10 (EXPA10), PLASMA MEMBRANE INTRINSIC PROTEIN*

1;4 (PIP1;4), and *IAA-leu-resistant-like 5 (ILL5). EXPA10* belongs to the expansin gene family whose members are able to induce cell wall loosening through a non-enzymatic function and have been implicated in plant-pathogen interactions.[47,48] *PIP1;4* is a plasma membrane localized aquaporin. Of the 13 *PIP* family members in *Arabidopsis*, 10 were significantly induced in clusters M4 and M5. Aquaporins are membrane channels that facilitate the transport of water and small neutral molecules (H_2O, H_2O_2, and CO_2).[49] *ILL5* is most similar to *ILL3*, which encodes an amidohydrolase, involved in converting indole-3-acetic acid (IAA) from an amino acid conjugate to a free form to increase auxin signaling.[50,51] All three markers displayed high expression in susceptibility clusters M4 and M5 (Figures 4A–4C, left; Figure S7B). *EXPA10* and *ILL5* had relatively weak expression in the transition cluster M3 and low expression in immune clusters M1 and M2 (Figures 4A and 4C). In contrast, *PIP1;4* was expressed in clusters M1–M3, but at a lower level than M4 and M5 (Figure 4B).

We examined the expression of two independent transgenic lines for each susceptibility marker after inoculation with *Pst* DC3000 and observed similar results for both lines (*pEXPA10::NLS-3xmCitrine*, *pPIP1;4::NLS-3xmCitrine*, *pILL5::NLS-3xmCitrine*; Figures 4A–4C and S6D–S6F). The *EXPA10* and *PIP1;4* transcriptional reporter lines exhibited low levels of expression in mock-inoculated plants and increasing levels of expression after inoculation, peaking at 72 hpi (Figures 4A, 4B, S6D, and S6E). A time course experiment was able to detect *EXPA10* induction at 10 h, but at a lower level than the 24, 48, or 72 hpi time points (Figures 4A, S6B, and S6D). The *ILL5* transcriptional reporter lines exhibited low levels of expression in mock-inoculated plants and increasing levels of expression, peaking at 48 hpi (Figures 4C and S6F). *ILL5* expression decreased slightly at 72 hpi but was still higher than 24 hpi (Figures 4C and S6F). Thus, the susceptible markers are activated after bacterial infection and strongly induced during later infection stages. These data highlight expression of susceptibility genes at later infection stages, consistent with the pseudotime trajectory.

Immune and susceptible marker genes exhibit diverse patterns of spatial expression

Bacteria exhibit heterogeneity in colonization of a leaf after both syringe and surface inoculation (Figures 1A and 3A). Our transcriptional reporter lines enabled us to probe marker gene expression with high sensitivity and at single-cell resolution. Therefore, we investigated where pathogen-responsive cells are spatially localized after surface inoculation with *Pst* DC3000. First, we examined expression of the *FRK1* immune marker gene at 24 hpi when it showed highest expression (Figure 3B). *FRK1* was rarely expressed in mock samples, but was frequently observed in cells surrounding substomatal cavities colonized by bacteria (Figure 5A; Video S1). *P. syringae* uses stomatal pores to enter the leaf interior and colonize the substomatal cavity early during infection.[52] We quantified confocal micrographs to determine the spatial localization of *FRK1* expressing cells. Ninety-one percent of cells expressing *FRK1* after *Pst* DC3000 inoculation surrounded substomatal cavities (Figure 5B). Next, we quantified the proximity of *FRK1* expressing cells to bacterial colonies. Seventy-five percent of *FRK1* expressing cells were proximal (<15 μm) to bacterial colonies (Figure 5C). These data demonstrate that *FRK1*, which is known to be one of

the earliest PTI marker genes, exhibits strong and specific expression at sites of bacterial invasion.

In contrast to *FRK1*, the *LipoP1* transcriptional reporter line exhibited dynamic changes in spatial expression patterns during the course of infection. *LipoP1* is expressed in guard cells, which flank stomatal pores, in the absence of pathogen infection (Figure 3C and S6C). At 24 hpi, 60% of *LipoP1*-expressing cells were proximal to bacterial colonies (<15 μm; Figure S7C). However, *LipoP1* exhibited variable spatial expression at 48 and 72 hpi, either generally induced in all cells or highly induced in cells surrounding bacterial colonies, possibly because of unsynchronized bacterial infection within different leaves. We analyzed the expression pattern of *LipoP1* over time using bacterial fluorescence intensity as a proxy for bacterial colony size. In particular, we observed two patterns of *LipoP1* expression in cells surrounding bacterial colonies: a robust expression pattern surrounding colonies with a fluorescence intensity less than 300 pixels/mm^2 (bundled pattern) as well as expression at the margins of larger colonies with a fluorescence intensity greater than 400 pixels/mm^2 (marginal expression, Figures 5D–5F). Bundled and marginal *LipoP1* expression patterns were significantly higher than in uncolonized regions (Figure S7D). Plant cells at the center of marginal pattern did not exhibit chlorophyll autofluorescence, which indicates they died because of severe bacterial colonization. Collectively, these results suggest different *LipoP1* expression patterns are associated with bacterial population size.

CPB60g encodes a master immune transcription factor that works in parallel with SARD1 to regulate the synthesis of the plant defense hormone SA.[44,53] In the absence of pathogen infection, *CBP60g* is generally expressed with low levels in all cells. After *Pst* DC3000 inoculation, the *CPB60g* transcriptional reporter line exhibited similar induction patterns to *LipoP1*, including general, bundled, and marginal patterns (Figures 5G and 5H). The general induction of *CPB60g* may be reflective of its role in SA biogenesis and transcriptional regulation of *NPR1*, which are critical for within-leaf and systemic immune responses.[44,53]

The intriguing spatial association of immune marker expression and bacterial colonization prompted us investigate if expression of susceptibility markers were spatially associated with bacterial colonization. We observed more broad induction of expression of the susceptibility marker *EXPA10* in large areas of the leaf that were proximal to regions robustly colonized by bacteria (Figure 5I), which contrasts with the more specific expression of the immune markers *FRK1*, *LipoP1*, and *CBP60g*. This *EXPA10* pattern of induction in sections of the leaf was most striking at 24 hpi before more uniform colonization of the leaf with larger bacterial colonies (Figures 3A and 5I). Reporter lines for *EXPA10* and *PIP1;4* exhibited detectable expression in epidermal and mesophyll cells in the absence of pathogen infection (Figure 4, S6E, and S6F). In contrast, *ILL5* was mainly expressed in guard cells in leaves without bacterial infection, but strongly induced at 48–72 hpi in epidermal, mesophyll, and guard cells (Figures 5J and 5K). Collectively, the transcriptional reporter lines representing immune and susceptible markers reveal distinct patterns of spatial and temporal expression during disease progression.

DISCUSSION

Plants respond to pathogen infection in a heterogeneous manner. Here, we revealed heterogeneity of plant responses at single-cell resolution using scRNA-seq coupled with confocal imaging of transcriptional reporter lines. Individual plant cells at immune, susceptible, or transition states highlighted the gradient of responses within an infected leaf. Immune markers exhibit diverse spatial and temporal expression patterns, while susceptible markers exhibit more expansive and sustained expression patterns in response to virulent *Pst* DC3000 (Figure 6). These data indicate that virulent bacteria are able to reprogram larger sections of the leaf toward susceptibility.

Our understanding of host-pathogen interactions is largely influenced by assays investigating whole-tissue samples. However, even after uniform inoculation, pathogens exhibit uneven penetration into the leaf interior and variable colonization within a tissue, which should result in variable host responses. For example, spores from the fungal pathogen *Zymoseptoria tritici* are able to continuously germinate on wheat leaves and their hyphae penetrate stomata for up to 10 days, resulting in multiple asynchronized infection stages at any given time.[4,5,54] *P. syringae* also exhibits uneven distribution on bean leaf surfaces, forming aggregates at leaf veins, crevices, trichomes, and occasionally stomata.[55] Similarly, we were able to visualize uneven colonization patterns of *Pst* DC3000 after syringe and surface inoculation on *Arabidopsis* (Figures 1A and 3A). Our scRNA-seq analyses were able to simultaneously identify cell clusters exhibiting opposing biological processes (immunity and susceptibility) at 24 hpi, indicating asynchronous infection stages even early during infection (Figure 2).

Although *Pst* DC3000 is virulent on *Arabidopsis*, the pathogen can still induce damage and carries MAMPs that can be perceived by plant PRRs (flagellin, elongation factor Tu and 3′OH fatty acid epitopes), resulting in localized immune-activated cell clusters. Previous research has found purified MAMP treatment can initiate transcriptional responses within 5 min and *Pst* DC3000 infiltration within 2 h.[56,57] The pseudotime trajectory of our scRNA-seq data placed the immunity cell clusters at an early stage of disease progression (Figure 2D). We identified two immune cell clusters (Figure 2), possibly due to waves of PTI transcriptional responses.[56] Consistent with these observations, our immune transcriptional reporter lines were also highly expressed at early infection time points (Figure 3). *FRK1* is a well-known early marker gene of PTI.[43,46,57] We found that *FRK1* expression was activated in cells surrounding substomatal cavities colonized by *Pst* DC3000 (Figures 3B and 5A–5C). *Pst* DC3000 uses stomatal pores to enter leaves and substomatal cavities are an early site of pathogen colonization.[52] Similarly, the highly induced immune markers *LipoP1* and *CBP60g* exhibited proximal expression to bacterial colonies during infection (Figures 5D–5H and S7C–S7E). The clustering of immune markers in cells surrounding bacteria may indicate that these bacterial colonies carry or create sufficient MAMPs/DAMPs to induce defense. A similar spatial expression pattern of the immune gene *PR1* was also observed around the infection site during effector-triggered immunity.[58,59] Compared with expression surrounding bacterial colonies, the immune marker *CBP60g* exhibited weaker, but general induction, in most cells at all infection stages, consistent with its role in inducing

SA synthesis whose accumulation is required for defense within a leaf as well as systemic immune responses (Figure 5G).[44,53]

Plant pathogens deliver effectors into host cells to dampen immune responses and promote susceptibility.[14,60] The timing and number of cells targeted for effector delivery also varies, but can occur within 75–90 min after bacterial infiltration on *Arabidopsis*.[61,62] Transcriptional profiling of *Arabidopsis* infected by virulent *Pst* DC3000 detected effector-mediated suppression of PTI and upregulation of genes contributing to susceptibility by 6 h.[57,63] Our scRNA-seq and promoter-reporter line investigations identified clusters of cells exhibiting patterns consistent with a compatible or susceptible interaction that peaked later during infection (Figures 2 and 4). For example, genes involved in water transport and ABA related processes were enriched in susceptible (M4 and M5) clusters. Recently, it has been reported that the HopM1 and AvrE effector family are responsible for apoplastic water-soaking phenotypes as a result of their ability to manipulate ABA signaling to induce stomatal closure.[64–66] Unlike the localized expression of immune markers, susceptibility markers exhibited more general expression, indicating more global reprogramming of the leaf to a susceptible state over time. The susceptibility markers *EXPA10* and *PIP1;4* encode members of gene families that function in cell wall enlargement/expansion and water transport under normal conditions, respectively.[47,49] During infection these processes can be manipulated by pathogens to create favorable environments for proliferation and disease development.[3,48]

Transcriptional profiling of entire tissues can mask cells at opposing response trajectories by averaging signals across thousands of cells. Comparing gene regulation in immune (M1 and M2) and susceptible (M4 and M5) clusters has resulted in the identification of candidates (Figures S4B–S5; Table S1C), including specific members of large gene families, involved in foliar plant-pathogen interactions. Genes regulating plant immune perception and signaling have been well characterized over the past 30 years, but identification of susceptibility genes has lagged behind.[67] Susceptibility genes are attractive targets to modify for developing disease resistant crops because of advances in genome editing technologies and decreased regulatory oversight.[60,68] Future advancements in high-resolution spatial transcriptomics enabling profiling of both plant and pathogen tissues, will facilitate investigating gene expression in a positional context in complex tissues.[33,69] Detailed characterization of cellular states throughout disease development will enable a comprehensive understanding of mechanisms regulating disease progression.

Limitations of the study

Plant scRNA-seq experiments require generating protoplasts, a process that will induce transcriptional changes. Although we controlled for protoplast induced genes, it is likely that some defense gene induction will not be detectable. A single scRNA-seq experiment was conducted per treatment on pooled samples of 10 plants each for mock treatment and 10 plants each for pathogen treatment.

STAR★METHODS

RESOURCE AVAILABILITY

Lead contact—Further information and requests for resources and reagents should be directed to and will be fulfilled by the lead contact, Gitta Coaker (glcoaker@ucdavis.edu).

Materials availability—Seeds of transgenic plants generated in this study are deposited in *Arabidopsis* Biological Research Center (ABRC, stock number: see key resources table). Plasmids used to generate transgenic plants are deposited in Addgene (Addgene ID: see key resources table).

Data and code availability

- Single-cell and bulk RNA-seq datasets generated in this study have been deposited at Gene Expression Omnibus (GSE213625). Original microscopy images have been deposited in Zenodo (https://doi.org/10.5281/zenodo.7686553).
- All original code has been deposited at Zenodo (https://doi.org/10.5281/zenodo.7888124).
- Any additional information required to reanalyze the data reported in this paper is available from the lead contact upon request.

EXPERIMENTAL MODEL AND STUDY PARTICIPANT DETAILS

Plant material and growth conditions—*Arabidopsis thaliana* ecotype Columbia Col-0 was used in single-cell RNA sequencing, bacterial growth curves and plant transformation. The transcriptional reporter line *pFRK1::NLS-3xmVENUS* in the Col-0 background was obtained from Professor Niko Geldner's lab.[46]

Arabidopsis thaliana seeds (Col-0 or transgenic lines) were stratified for 2 days in the dark at 4°C before sowing onto soil or half-strength (1/2) Murashige and Skoog (MS) medium. Seeds were also surface-sterilized with disinfection solution (50% Bleach, 0.1% Tween 20) for 8 min and 75% ethanol for 1 min, washed thoroughly in sterile water for 4 times before sowing onto 1/2 MS medium. Four-week-old *A. thaliana* Col-0 used for scRNA-seq and plant transformation were grown in a controlled environment chamber at 22°C and 70% relative humidity with 10 h light/14 h dark photoperiod (100 μM m^{-2} s^{-1}). Ten to 14-day-old seedlings grown on 1/2 MS were incubated at 22°C under long-day conditions with 16 h light/8 h dark cycles. Seedlings were used for microscopy analyses.

Bacterial strains and growth conditions—*Pseudomonas syringae pv. tomato* DC3000 *ΔhopQ1* and wild-type *Pst* DC3000 were labeled with 3xmCherry (*att*Tn7-3xmCherry, *Pst* DC3000-mCherry) using the site-specific Tn7 3xmCherry vector.[70] Tn7 3xmCherry was transformed into competent cells of *Pseudomonas syringae* by electroporation. Cell suspensions were plated on nutrient yeast glycerol agar NYGA medium containing 100 μg/mL of rifampicin and 50 μg/mL of spectinomycin. After incubating two days at 28°C, bacterial colonies were screened. For all inoculations, bacteria were cultured overnight

at 28°C on NYGA medium containing 100 μg/mL of rifampicin and 50 μg/mL of spectinomycin.

METHOD DETAILS

Bacterial inoculation and quantification—Cells from an overnight culture of *Pst* DC3000-3xmCherry or *Pst* DC3000 *ΔhopQ1*-3xmCherry were collected and resuspended in 10 mM $MgCl_2$. For scRNA-seq, protoplast bulk RNA-seq, leaf bulk RNA-seq samples, and bacterial growth curves, leaves of four-week-old *A. thaliana* were syringe infiltrated with a bacterial suspension of OD_{600} = 0.0001. Inoculated plants were kept under ambient humidity for 1 h to allow evaporation of excess water on the leaf surface. Then plants were covered with a transparent dome to maintain high humidity and incubated in growth chamber for 24 h. For seedling flood inoculation, two-week-old plants on ½ MS medium were flood inoculated using 40 mL of the bacterial suspension of OD_{600} = 0.01 with 0.02% Silwet L-77 per 100 mm x 100 mm square petri dish (Fisherbrand). The bacterial suspension was removed after 20-30 s incubation at room temperature. Inoculated plants were sealed with 3 M Micropore tape (3 M, St. Paul, MN, U.S.A.) and incubated in a growth chamber.

Bacterial titers after flood inoculation were determined as colony-forming units (CFU) per milligram. In brief, three plants were cut roots away as one biological repeat, and 5-7 repeats were taken for each time. After measuring the weight of the aerial parts of each repeat, samples were ground and diluted in 5 mM $MgCl_2$. The bacterial suspensions were then plated on (NYGA) medium containing 100 μg/mL of rifampicin. Colonies were counted at each time point after incubation at 28°C. Bacterial titers after syringe infiltration were determined as described previously.[71] Briefly, one leaf disk was taken from one inoculated plant using a cork borer (6 mm in diameter) and ground in 400 μl of 5 mM $MgCl_2$. This served as one repeat, and 5-7 repeats were performed for each experiment. The bacterial suspensions were then diluted and plated on NYGA medium containing 100 μg/mL of rifampicin. Colonies were counted at each time point after incubation at 28°C.

Protoplast isolation—Protoplasts were isolated from *Arabidopsis* leaves infiltrated by bacteria and 10 mM $MgCl_2$ (Mock) using Tape-*Arabidopsis* Sandwich method as described previously.[30] The adaxial side of 10-20 infiltrated leaves (from 10 plants) for each treatment was stabilized on the time tape and the abaxial side was adhered to the Magic tape (3M). The abaxial side was removed by carefully pulling off the Magic tape. Peeled leaves were immediately immersed in a petri dish containing 10 mL of enzyme solution (1.5% Cellulase Onuzuka R-10 (Yakult, Japan), 0.3% Macerozyme R-10, (Yakult, Japan), 0.4 M Mannitol, 20 mM KCl, 20 mM MES (2-(N-Morpholino)ethanesulfonic acid hydrate) pH 5.7, 10 mM $CaCl_2$, and 0.1% BSA). After digesting for 100 min with gentle shaking, the protoplast suspension was filtered through 40 μm cell strainer (BD Falcon 352340) into a round-bottomed 50 mL tube and centrifuged at 100x g for 1 min at 22°C using a swinging rotor. Protoplast pellets were gently resuspended in 10 mL of CS-sucrose buffer (0.4 M sucrose, 20 mM MES pH 5.7, 20 mM KCl) and centrifuged at 100x g for 2 min at 22°C. Intact and healthy protoplasts remained suspended in the upper layer. The upper layer suspension was then transferred into a clean round-bottomed tube and gently mixed with 10 mL of protoplast buffer (0.4 M Mannitol, 20 mM KCl, 20 mM MES pH 5.7, and 0.1% BSA). After

centrifuging at 100x g for 2 min at 4°C using a swinging rotor, the supernatant was removed without disturbing the loosely packed protoplast pellets. The protoplast concentration was determined using a hemocytometer and the viability was checked using trypan blue solution. The protoplast sample from each treatment (DC3000 and mock) was divided for scRNA-seq and bulk RNA-seq.

scRNA-seq library preparation and sequencing—The protoplast suspension was diluted to a final concentration of 1000 cells/μL. A total of 40, 000 cells were loaded into a microfluidic chip (10X Genomics) with v3 chemistry to capture ~10,000 cells per sample. Protoplasts were barcoded with a Chromium Controller (10X Genomics). mRNA was reverse transcribed and cDNA libraries were constructed with a Chromium Single Cell 3' reagent kit V3 (10X Genomics) according to the manufacturer's instructions. Eleven cycles were used for cDNA amplification and 10 cycles were used for final library amplification. cDNA and final library quality was assessed using a Bioanalyzer 2100 High Sensitivity DNA Chip (Agilent). Sequencing of paired-end 150 bp reads was performed with a NovaSeq 6000 instrument (Illumina) at the University of California Davis Genome Center. Protoplasts from DC3000 treatment and mock inoculation were each barcoded on a single Chromium Controller.

RNA extraction, bulk RNA-seq library preparation and sequencing—Total RNA was extracted with TRIzol (Fisher #15596018), following the manufacturer's instructions, for intact infiltrated leaves as well as leaf protoplasts isolated using the above mentioned method for scRNA-seq. DNase treatments were performed with RQ1 RNase-Free DNase (Promega #PR-M6101). Three biological replicates were performed for samples of *Pst* DC3000- or mock-infiltrated leaves, and one repeat was made for leaf protoplasts of each sample. cDNA libraries were prepared with QuantSeq FWD kit (Lexogen), according to the manufacturer's protocol. The fragment size distribution was evaluated by a Bioanalyzer 2100 (Agilent). The library pool was treated using Exonuclease VII (NEB), SPRI-bead purified with KapaPure beads (Kapa Biosystems /Roche), quantified via qPCR with a Kapa Library Quant kit (Kapa Biosystems) on a QuantStudio 5 RT-PCR system (Applied Biosystems). Sequencing was performed at the University of California Davis Genome Center using a HiSeq 4000 (Illumina) platform with single-end 100 bp reads.

Bulk RNA-seq data analysis—Raw fastq files for three bulk RNA-seq replicates each for *Pst* DC3000- and mock-inoculated leaves, as well as one bulk RNA-seq replicate from protoplasts isolated from *Pst* DC3000- and mock-inoculated leaves were trimmed using TrimGalore (stringency = 4, default parameters otherwise) and aligned to the *Arabidopsis thaliana* reference genome (Araport11) and quantified using STAR. Differential expression metrics for protoplasting and bacterial-induced changes were evaluated using the glmQLFit method from the edgeR package (Bioconductor v3.12), using a design matrix that takes into consideration the interaction between these two variables. Genes determined to be significantly altered by protoplasting were identified using a relatively liberal set of criteria, i.e. having log-fold change values > 0.5 and adjusted (BH) p-values less than 0.05, and were removed from dimension reduction and integration analyses. Genes determined to be

significantly affected by *Pst* DC3000 were those having log-fold change values >2 and adjusted (BH) p values less than 0.01, unless otherwise specified.

scRNA-seq data initial processing and integration—Raw fastq files for the two samples generated in this study (Mock, *Pst* DC3000) were processed using Cellranger (v6.0.1; 10x Genomics, Pleasanton, CA) using default parameters (and an expected cell # equal to 10,000), mapping to the Araport11 *Arabidopsis* reference genome. The output from Cellranger was further processed using the Velocyto (v0.17.15) algorithm,[72] using default parameters, to generate spliced and unspliced counts matrices. For each cell, the percentage of reads mapping to mitochondrial, and chloroplast genes was computed. Cells were then filtered for those having a spliced mitochondrial read percentage of less than 1%, as well as a total spliced Unique Molecular Identifier (UMI) count within a dataset dependent threshold, bounded at the high end by 50,000 counts, and at the low end by 10% of the UMI count of the 100th most spliced transcript-rich cell for that dataset.[73]

Cells were normalized using the SCTransform method (Seurat, v3.9.9005). A recent *Arabidopsis* leaf single-cell RNA-seq dataset[23] was used to annotate cell types for all cells in this dataset using the label transfer pipeline (Seurat). Genes that were identified as being significantly influenced by protoplasting (see Bulk RNA-seq data analysis) were excluded from further analysis.

The *Pst* DC3000 and mock-inoculated datasets were then integrated using the anchor method (Seurat). Fifty principal components were calculated for the integrated dataset, used to cluster the cells (Louvain method, resolution 0.8) and further dimensionally reduce the gene expression space using Uniform Manifold Approximation and Projection (Seurat), using 50 Principal Components and default parameters (Table S2).

Pseudobulk analysis—A pseudobulk value for each gene was calculated as the sum of all counts from all cells for that gene within either the Mock- or *Pst* 3000-treated single-cell datasets. These values were then used to compare against whole-tissue or pooled-protoplast bulk RNA-seq data to verify that the single-cell datasets coarsely resemble bulk RNA-seq datasets.

Signature score computation—A *Pst* DC3000 signature score was computed as a composite metric quantifying the overall impact that *P. syringae* has on each cell. Here, the Seurat AddModuleScore function was used to define a pair of module score for genes up- or down-regulated by *Pst* DC3000 (from bulk RNA-seq data), with the signature score defined as the *Pst* DC3000-up module score subtracted from the *Pst* DC3000-down module score. Similarly, an Immunity Response Score was defined as a composite signature score quantifying the general state that each cell was in with respect to disease progression based on sets of genes known to be induced/involved in immune response (Immunity) and in advanced disease (Susceptibility). These genes were filtered for those that were found to be differentially expressed from our bulk RNA-seq analysis (see above). Immune and Susceptibility module scores were then computed using the AddModuleScore function (Seurat), and the Response Score was defined as the Susceptibility score subtracted from the Immunity score. Similarly, we also generated a protoplast signature score for those genes

induced or repressed by protoplasting, generating another compound signature score for the overall effect of protoplasting (Figure S2)

Cluster-specific marker loci—Marker genes specifically expressed in each cell cluster were determined using the FindAllMarkers function (Seurat) (Table S1D). Significant markers were defined as those having a log-fold change (compared to all other clusters) greater than 0.25, and an adjusted (BH) p-value (wilcoxon rank sum test) less than 0.01. Log-fold change values between Mock- and *Pst* 3000-treated single-cell transcriptomes were computed for all superclusters (Immunity, Susceptibility, Transition, etc.) using the FindMarkers function (Seurat), with significance calculated using the DESeq2 (v1.30.1) method on the unnormalized counts.

GO term enrichment—For each cluster, a stringent set of marker loci was computed using the FindAllMarkers function in Seurat. GO term enrichment analysis was then performed using the topGO R package (Bioconductor version 3.12) for these marker genes, using all expressed genes (excluding those induced by protoplasting) as background. GO enrichment was calculated as the number of significant genes divided by the number of expected genes for each GO term.

Pseudotime inference—SCTransform-normalized expression values for spliced transcripts in mesophyll cells (excluding Seurat cluster 16, which seemed distinct from other mesophyll cells) were filtered from the *Pst* DC3000 dataset and re-embedded in a low-dimensional UMAP space using the Monocle 3 (v1.0.0) pipeline (using 5 principal components, the correlation distance metric, and a minimum distance of 0.01). A cell trajectory was then imputed using Monocle 3, defining the starting cell as that with the lowest *Pst* DC3000-expression score (a measure of how influenced the cell is by pathogen expression, empirically determined using bulk RNA-seq expression data) within the cluster with the lowest mean *Pst* DC3000 signature score, and a minimum branch length of 15. Pseudotime was projected onto this cell trajectory for *Pst* DC3000 mesophyll cells. Genes that vary significantly with pseudotime were computed with the graph_test function (Monocle 3), using “principal graph” as the neighbor_graph parameter. Genes were selected as significant as those having a Morans I value greater than 0.2 (Table S1C).

Generation of transgenic lines—Genes for the generation of reporter lines were selected based on their enrichment in clusters M1-M5 (adjusted p-value from the FindAllMarkers Seurat function less than 0.01, and a log-fold change greater than 1), relatively specific expression from scRNA-seq analyses in either immune or susceptible clusters and potentially interesting functions from the literature. Promoters (~ 2 kb upstream of the start codon) of *LipoP1* (AT3G18250, 2210 bp), *CBP60g* (AT5G26920, 2183 bp), *EXPA10* (AT1G26770, 2025 bp), *PIP1;4* (AT4G00430, 2151 bp) and *ILL5* (AT1G51780, 2089 bp) were PCR-amplified and fused to a nuclear localization signal (NLS) in pENTR vectors using In-Fusion HD Cloning Plus (Clontech). See Table S3 for primer details. The resulting constructs were recombined with binary destination vector pMpGWB123[74] bearing 3xmCitrine using Gateway Cloning Technology (Invitrogen). All plasmids were transformed into *Agrobacterium tumefaciens* GV3101 strain and then transformed into *A. thaliana* Col-0

by floral dipping method.[75] Seedlings of transgenic plants were screened on ½ MS plates supplemented with 25 μg/mL of hygromycin and 100 μg/mL of carbenicillin. Ten to fifteen independent T1 lines were analyzed for mCitrine fluorescence, and 3-5 T2 lines expressing mCitrine were selected for bacterial infection. Transgenic plants T2 or T3 (1-2 independent lines) with similar induction patterns after bacterial infection were selected for further experiments.

Confocal settings and image processing—Confocal imaging was performed on either a Leica TCS SP8 or Zeiss LSM 980 with Airyscan 2 laser scanning microscope. Pictures were taken with a 20x (Leica TCS SP8 or Zeiss LSM 980), 10x dry immersion objectives (Leica TCS SP8), as well as 5x immersion objective for tile-scan with 10% overlap (Leica TCS SP8). The following excitation and emission parameters were used for different fluorophores: mVENUS/mCitrine 488 nm, 493 – 540 nm; mCherry 552 nm, 586 – 635 nm; chlorophyll 638 nm, 650 -720 nm on Leica TCS SP8. mCitrine 488 nm, 490 – 543 nm; mCherry 561nm, 570 – 640 nm on Zeiss LSM 980. Sequential scanning was applied to avoid fluorescence interference between channels. Time-course confocal images of each transcriptional reporter line were taken under identical settings (lens, laser power, pinhole size, detector gain, and interval of Z stack) for comparison of fluorescence intensity over time. Different microscope settings were applied for different transcriptional reporter lines according to the expression level of transgenes in plants.

Quantification of bacterial colony number, area, and fluorescence intensity was performed with the Imaris software (https://imaris.oxinst.com/). In brief, the Surface Model tool was used to quantify colony number and area of an entire image. Background subtraction was used to manually adjust threshold until all visible fluorescently-labeled bacteria colonies were detected. Then the detected colonies were counted and surface area measured. The Spot tool was used to build spots for each fluorescence domain to quantify fluorescence intensity. Quantification was determined by measurement of mean fluorescence intensity per spot (fluorescence intensity/nucleus). Algorithm settings of Different Spot Sizes were used due to variable nuclei size in different cell types of plant leaves. Background subtraction function was used for spot detection. To classify spots, “Quality (pixel intensity of a spot center)” filter was used to manually adjust threshold until all visible fluorescently-labeled nuclei were detected. Spot regions were determined by manually adjusting threshold of absolute intensity detection to ensure complete coverage of fluorescently-labeled nuclei.

QUANTIFICATION AND STATISTICAL ANALYSIS

Statistical analyses were performed with Graphpad Prism 9.0 software (https://www.graphpad.com/) or in R. The data are presented as mean ± SD, and “n” represents number of analyzed images from at least 3 plants. One-way ANOVA with Tukey’s test was used for multiple comparisons. Two tailed Student’s t-test was used to compare means for two groups. Details about the statistical analyses are described in the figure legends.

Supplementary Material

Refer to Web version on PubMed Central for supplementary material.

ACKNOWLEDGMENTS

We thank Dr. Niko Geldner (University of Lausanne) for providing *FRK1* transcriptional reporter seeds, Dr. Lei Lei (Lanzhou University) for bulk RNA extraction from leaves, and Dr. Pamela Ronald (University of California [UC], Davis) for use of their confocal microscope. We also would like to thank all the members of Coaker lab for helpful discussions and input on the project. This work was supported by a grant to G.C. from the NIH (R35GM136402). S.L. was supported by the Independent research fund Denmark (grant 7026-00053B). The work conducted by the U.S. Department of Energy Joint Genome Institute (https://ror.org/04xm1d337), a DOE Office of Science User Facility, was supported by the Office of Science of the U.S. Department of Energy operated under contract DE-AC02-05CH11231. B.K. was supported by a U.S. Department of Agriculture (USDA) National Institute of Food and Agriculture (NIFA) award (2017-67030-25920). The sequencing was carried out at the UC Davis Genome Center DNA Technologies and Expression Analysis Core, supported by an NIH Shared Instrumentation Grant (1S10OD010786-01). The graphical abstract was created using BioRender.com.

REFERENCES

1. Berruyer R, Poussier S, Kankanala P, Mosquera G, and Valent B (2006). Quantitative and qualitative influence of inoculation methods on in planta growth of rice blast fungus. Phytopathology 96, 346–355. 10.1094/phyto-96-0346. [PubMed: 18943416]
2. Pétriacq P, Stassen JHM, and Ton J (2016). Spore density determines infection strategy by the plant pathogenic fungus *Plectosphaerella cucumerina*. Plant Physiol. 170, 2325–2339. 10.1104/pp.15.00551. [PubMed: 26842622]
3. Xin XF, Nomura K, Aung K, Velásquez AC, Yao J, Boutrot F, Chang JH, Zipfel C, and He SY (2016). Bacteria establish an aqueous living space in plants crucial for virulence. Nature 539, 524–529. 10.3410/f.727018704.793526211. [PubMed: 27882964]
4. Fantozzi E, Kilaru S, Gurr SJ, and Steinberg G (2021). Asynchronous development of *Zymoseptoria tritici* infection in wheat. Fungal Genet. Biol 146, 103504. 10.1016/j.fgb.2020.103504. [PubMed: 33326850]
5. Haueisen J, Möller M, Eschenbrenner CJ, Grandaubert J, Seybold H, Adamiak H, and Stukenbrock EH (2019). Highly flexible infection programs in a specialized wheat pathogen. Ecol. Evol 9, 275–294, 10.1002/ece3.4724. 10.1002/ece3.4724. [PubMed: 30680113]
6. Matsumoto A, Schlüter T, Melkonian K, Takeda A, Nakagami H, and Mine A (2022). A versatile Tn7 transposon-based bioluminescence tagging tool for quantitative and spatial detection of bacteria in plants. Plant Commun. 3, 100227. 10.1101/2021.02.11.430857. [PubMed: 35059625]
7. Katagiri F, Thilmony R, and He SY (2002). The *Arabidopsis thaliana-pseudomonas syringae* interaction. Arabidopsis Book 1, e0039, 10.1199/tab.0039. 10.1199/tab.0039. [PubMed: 22303207]
8. Xin X-F, Kvitko B, and He SY (2018). *Pseudomonas syringae*: what it takes to be a pathogen. Nat. Rev. Microbiol 16, 316–328. 10.1038/nrmicro.2018.17. [PubMed: 29479077]
9. Bigeard J, Colcombet J, and Hirt H (2015). Signaling mechanisms in pattern-triggered immunity (PTI). Mol. Plant 8, 521–539. 10.1016/j.molp.2014.12.022. [PubMed: 25744358]
10. Wang Y, Tyler BM, and Wang Y (2019). Defense and counterdefense during plant-pathogenic oomycete infection. Annu. Rev. Microbiol 73, 667–696. 10.1146/annurev-micro-020518-120022. [PubMed: 31226025]
11. Yuan M, Ngou BPM, Ding P, and Xin X-F (2021). PTI-ETI crosstalk: an integrative view of plant immunity. Curr. Opin. Plant Biol 62, 102030. 10.1016/j.pbi.2021.102030. [PubMed: 33684883]
12. Lolle S, Stevens D, and Coaker G (2020). Plant NLR-triggered immunity: from receptor activation to downstream signaling. Curr. Opin. Immunol 62, 99–105. 10.1016/j.coi.2019.12.007. [PubMed: 31958770]
13. Zhou JM, and Zhang Y (2020). Plant immunity: danger perception and signaling. Cell 181, 978–989. 10.1016/j.cell.2020.04.028. [PubMed: 32442407]
14. Toruño TY, Stergiopoulos I, and Coaker G (2016). Plant-pathogen effectors: cellular probes interfering with plant defenses in spatial and temporal manners. Annu. Rev. Phytopathol 54, 419–441. 10.1146/annurev-phyto-080615-100204. [PubMed: 27359369]
15. Liu Z, Hou S, Rodrigues O, Wang P, Luo D, Munemasa S, Lei J, Liu J, Ortiz-Morea FA, Wang X, et al. (2022). Phytocytokine signalling reopens stomata in plant immunity and water loss. Nature 605, 332–339. 10.1038/s41586-022-04684-3. [PubMed: 35508659]

16. Zipfel C, Kunze G, Chinchilla D, Caniard A, Jones JDG, Boller T, and Felix G (2006). Perception of the bacterial PAMP EF-Tu by the receptor EFR restricts *Agrobacterium*-mediated transformation. Cell 125, 749–760. 10.1016/j.cell.2006.03.037. [PubMed: 16713565]

17. Kolodziejczyk AA, Kim JK, Svensson V, Marioni JC, and Teichmann SA (2015). The technology and biology of single-cell RNA sequencing. Mol. Cell 58, 610–620. 10.1080/15476286.2016.1201618. [PubMed: 26000846]

18. Libault M, Pingault L, Zogli P, and Schiefelbein J (2017). Plant systems biology at the single-cell level. Trends Plant Sci. 22, 949–960. 10.1016/j.tplants.2017.08.006. [PubMed: 28970001]

19. Macosko EZ, Basu A, Satija R, Nemesh J, Shekhar K, Goldman M, Tirosh I, Bialas AR, Kamitaki N, Martersteck EM, et al. (2015). Highly parallel genome-wide expression profiling of individual cells using nanoliter droplets. Cell 161, 1202–1214. 10.3410/fi725508338.793543121. [PubMed: 26000488]

20. Tang F, Barbacioru C, Wang Y, Nordman E, Lee C, Xu N, Wang X, Bodeau J, Tuch BB, Siddiqui A, et al. (2009). mRNA-Seq whole-transcriptome analysis of a single cell. Nat. Methods 6, 377–382. 10.1038/nmeth.1315. [PubMed: 19349980]

21. Seyfferth C, Renema J, Wendrich JR, Eekhout T, Seurinck R, Vandamme N, Blob B, Saeys Y, Helariutta Y, Birnbaum KD, and De Rybel B (2021). Advances and opportunities in single-cell transcriptomics for plant research. Annu. Rev. Plant Biol 72, 847–866. 10.1146/annurev-arplant-081720-010120. [PubMed: 33730513]

22. Denyer T, Ma X, Klesen S, Scacchi E, Nieselt K, and Timmermans MCP (2019). Spatiotemporal developmental trajectories in the *Arabidopsis* root revealed using high-throughput single-cell RNA sequencing. Dev. Cell 48, 840–852.e5. 10.1016/j.devcel.2019.02.022. [PubMed: 30913408]

23. Kim J-Y, Symeonidi E, Pang TY, Denyer T, Weidauer D, Bezrutczyk M, Miras M, Zöllner N, Hartwig T, Wudick MM, et al. (2021). Distinct identities of leaf phloem cells revealed by single cell transcriptomics. Plant Cell 33, 511–530. 10.1093/plcell/koaa060. [PubMed: 33955487]

24. Lopez-Anido CB, Vatén A, Smoot NK, Sharma N, Guo V, Gong Y, Anleu Gil MX, Weimer AK, and Bergmann DC (2021). Single-cell resolution of lineage trajectories in the *Arabidopsis* stomatal lineage and developing leaf. Dev. Cell 56, 1043–1055.e4. 10.1016/j.devcel.2021.03.014. [PubMed: 33823130]

25. Procko C, Lee T, Borsuk A, Bargmann BOR, Dabi T, Nery JR, Estelle M, Baird L, O'Connor C, Brodersen C, et al. (2022). Leaf cell-specific and single-cell transcriptional profiling reveals a role for the palisade layer in UV light protection. Plant Cell 34, 3261–3279. 10.1093/plcell/koac167. [PubMed: 35666176]

26. Shahan R, Hsu C-W, Nolan TM, Cole BJ, Taylor IW, Greenstreet L, Zhang S, Afanassiev A, Vlot AHC, Schiebinger G, et al. (2022). A single-cell *Arabidopsis* root atlas reveals developmental trajectories in wild-type and cell identity mutants. Dev. Cell 57, 543–560.e9. 10.1016/j.devcel.2022.01.008. [PubMed: 35134336]

27. Zhang T-Q, Chen Y, and Wang J-W (2021). A single-cell analysis of the *Arabidopsis* vegetative shoot apex. Dev. Cell 56, 1056–1074.e8. 10.1016/j.devcel.2021.02.021. [PubMed: 33725481]

28. Wei CF, Kvitko BH, Shimizu R, Crabill E, Alfano JR, Lin NC, Martin GB, Huang HC, and Collmer A (2007). A *Pseudomonas syringae* pv. tomato DC3000 mutant lacking the type III effector HopQ1-1 is able to cause disease in the model plant *Nicotiana benthamiana*. Plant J. 51, 32–46. 10.1111/j.1365-313x.2007.03126.x. [PubMed: 17559511]

29. Whalen MC, Innes RW, Bent AF, and Staskawicz BJ (1991). Identification of *Pseudomonas syringae* pathogens of *Arabidopsis* and a bacterial locus determining avirulence on both *Arabidopsis* and soybean. Plant Cell 3, 49–59. 10.2307/3869199. [PubMed: 1824334]

30. Wu F-H, Shen S-C, Lee L-Y, Lee S-H, Chan M-T, and Lin C-S (2009). Tape-*Arabidopsis* Sandwich-a simpler *Arabidopsis* protoplast isolation method. Plant Methods 5, 16–10. 10.1186/1746-4811-5-16. [PubMed: 19930690]

31. Liu Z, Zhou Y, Guo J, Li J, Tian Z, Zhu Z, Wang J, Wu R, Zhang B, Hu Y, et al. (2020). Global dynamic molecular profiling of stomatal lineage cell development by single-cell RNA sequencing. Mol. Plant 13, 1178–1193. 10.1016/j.molp.2020.06.010. [PubMed: 32592820]

32. Zhang TQ, Xu ZG, Shang GD, and Wang JW (2019). A single-cell RNA sequencing profiles the developmental landscape of *Arabidopsis* root. Mol. Plant 12, 648–660. 10.1016/j.molp.2019.04.004. [PubMed: 31004836]
33. Saarenpää S, Shalev O, Ashkenazy H, de Oliveira-Carlos V, Lundberg DS, Weigel D, and Giacomello S (2022). Spatially Resolved Host-Bacteria-Fungi Interactomes via Spatial Metatranscriptomics, bio-Rxiv. 10.1101/2022.07.18.496977.
34. Cheong YH, Chang H-S, Gupta R, Wang X, Zhu T, and Luan S (2002). Transcriptional profiling reveals novel interactions between wounding, pathogen, abiotic stress, and hormonal responses in *Arabidopsis*. Plant Physiol. 129, 661–677. 10.1104/pp.002857. [PubMed: 12068110]
35. Reymond P, Weber H, Damond M, and Farmer EE (2000). Differential gene expression in response to mechanical wounding and insect feeding in *Arabidopsis*. Plant Cell 12, 707–720. 10.2307/3870996. [PubMed: 10810145]
36. Zheng XY, Spivey NW, Zeng W, Liu P-P, Fu ZQ, Klessig DF, He SY, and Dong X (2012). Coronatine promotes *Pseudomonas syringae* virulence in plants by activating a signaling cascade that inhibits salicylic acid accumulation. Cell Host Microbe 11, 587–596. 10.1016/j.chom.2012.04.014. [PubMed: 22704619]
37. Trapnell C, Cacchiarelli D, Grimsby J, Pokharel P, Li S, Morse M, Lennon NJ, Livak KJ, Mikkelsen TS, and Rinn JL (2014). The dynamics and regulators of cell fate decisions are revealed by pseudotemporal ordering of single cells. Nat. Biotechnol 32, 381–386. 10.1038/nbt.2859. [PubMed: 24658644]
38. Cao J, Spielmann M, Qiu X, Huang X, Ibrahim DM, Hill AJ, Zhang F, Mundlos S, Christiansen L, Steemers FJ, et al. (2019). The single-cell transcriptional landscape of mammalian organogenesis. Nature 566, 496–502. 10.1038/s41586-019-0969-x. [PubMed: 30787437]
39. Qiu X, Hill A, Packer J, Lin D, Ma Y-A, and Trapnell C (2017). Single-cell mRNA quantification and differential analysis with Census. Nat. Methods 14, 309–315. 10.1038/nmeth.4150. [PubMed: 28114287]
40. Qiu X, Mao Q, Tang Y, Wang L, Chawla R, Pliner HA, and Trapnell C (2017). Reversed graph embedding resolves complex single-cell trajectories. Nat. Methods 14, 979–982. 10.1038/nmeth.4402. [PubMed: 28825705]
41. Ishiga Y, Ishiga T, Uppalapati SR, and Mysore KS (2011). *Arabidopsis* seedling flood-inoculation technique: a rapid and reliable assay for studying plant-bacterial interactions. Plant Methods 7, 32–12. 10.1186/1746-4811-7-32. [PubMed: 21978451]
42. Asai T, Tena G, Plotnikova J, Willmann MR, Chiu W-L, Gomez-Gomez L, Boller T, Ausubel FM, and Sheen J (2002). MAP kinase signalling cascade in *Arabidopsis* innate immunity. Nature 415, 977–983. 10.1038/415977a. [PubMed: 11875555]
43. He P, Shan L, Lin N-C, Martin GB, Kemmerling B, Nürnberger T, and Sheen J (2006). Specific bacterial suppressors of MAMP signaling upstream of MAPKKK in Arabidopsis innate immunity. Cell 125, 563–575. 10.1016/j.cell.2006.02.047. [PubMed: 16678099]
44. Kim JH, Castroverde CDM, Huang S, Li C, Hilleary R, Seroka A, Sohrabi R, Medina-Yerena D, Huot B, Wang J, et al. (2022). Increasing the resilience of plant immunity to a warming climate. Nature 607, 339–344. 10.1038/s41586-022-04902-y. [PubMed: 35768511]
45. Zhang Y, Xu S, Ding P, Wang D, Cheng YT, He J, Gao M, Xu F, Li Y, Zhu Z, et al. (2010). Control of salicylic acid synthesis and systemic acquired resistance by two members of a plant-specific family of transcription factors. Proc. Natl. Acad. Sci. USA 107, 18220–18225. 10.1073/pnas.1005225107. [PubMed: 20921422]
46. Zhou F, Emonet A, Dénervaud Tendon V, Marhavy P, Wu D, Lahaye T, and Geldner N (2020). Co-Incidence of damage and microbial patterns controls localized immune responses in roots. Cell 180, 440–453.e18. 10.1016/j.cell.2020.01.013. [PubMed: 32032516]
47. Cosgrove DJ (2015). Plant expansins: diversity and interactions with plant cell walls. Curr. Opin. Plant Biol 25, 162–172. 10.1016/j.pbi.2015.05.014. [PubMed: 26057089]
48. Ding X, Cao Y, Huang L, Zhao J, Xu C, Li X, and Wang S (2008). Activation of the indole-3-acetic acid-amido synthetase GH3-8 suppresses expansin expression and promotes salicylate- and jasmonate-independent basal immunity in rice. Plant Cell 20, 228–240. 10.1105/tpc.107.055657. [PubMed: 18192436]

49. Maurel C, Boursiac Y, Luu D-T, Santoni V, Shahzad Z, and Verdoucq L (2015). Aquaporins in plants. Physiol. Rev 95, 1321–1358. 10.1152/physrev.00008.2015. [PubMed: 26336033]
50. Casanova-Sáez R, and Voß U (2019). Auxin metabolism controls developmental decisions in land plants. Trends Plant Sci. 24, 741–754. 10.1016/j.tplants.2019.05.006. [PubMed: 31230894]
51. Hayashi KI, Arai K, Aoi Y, Tanaka Y, Hira H, Guo R, Hu Y, Ge C, Zhao Y, Kasahara H, and Fukui K (2021). The main oxidative inactivation pathway of the plant hormone auxin. Nat. Commun 12, 6752. 10.1038/s41467-021-27020-1. [PubMed: 34811366]
52. Melotto M, Underwood W, and He SY (2008). Role of stomata in plant innate immunity and foliar bacterial diseases. Annu. Rev. Phytopathol 46, 101–122. 10.1146/annurev.phyto.121107.104959. [PubMed: 18422426]
53. Sun T,Zhang Y,Li Y,Zhang Q,Ding Y, andZhang Y(2015).ChIP-seq reveals broad roles ofSARD1 and CBP60g in regulating plant immunity. Nat. Commun 6, 10159–10212. 10.1038/ncomms10159. [PubMed: 27206545]
54. Fones HN, Eyles CJ, Kay W, Cowper J, and Gurr SJ (2017). A role for random, humidity-dependent epiphytic growth prior to invasion of wheat by Zymoseptoria tritici. Fungal Genet. Biol 106, 51–60. 10.1016/j.fgb.2017.07.002. [PubMed: 28694096]
55. Björklöf K, Nurmiaho-Lassila E, Klinger N, Haahtela K, and Romantschuk M (2000). Colonization strategies and conjugal gene transfer of inoculated Pseudomonas syringae on the leaf surface. J. Appl. Microbiol 89, 423–432. 10.1046/j.1365-2672.2000.01130.x. [PubMed: 11021574]
56. Bjornson M, Pimprikar P, Nürnberger T, and Zipfel C (2021). The transcriptional landscape of Arabidopsis thaliana pattern-triggered immunity. Native Plants 7, 579–586. 10.1038/s41477-021-00874-5.
57. Lewis LA, Polanski K, de Torres-Zabala M, Jayaraman S, Bowden L, Moore J, Penfold CA, Jenkins DJ, Hill C, Baxter L, et al. (2015). Transcriptional dynamics driving MAMP-triggered immunity and pathogen effector-mediated immunosuppression in Arabidopsis leaves following infection with Pseudomonas syringae pv tomato DC3000. Plant Cell 27, 3038–3064. 10.1105/tpc.15.00471. [PubMed: 26566919]
58. Betsuyaku S, Katou S, Takebayashi Y, Sakakibara H, Nomura N, and Fukuda H (2018). Salicylic acid and jasmonic acid pathways are activated in spatially different domains around the infection site during effector-triggered immunity in Arabidopsis thaliana. Plant Cell Physiol. 59, 8–16. 10.1093/pcp/pcx181. [PubMed: 29177423]
59. Jacob P, Hige J, Song L, Bayless A, Russ D, Bonardi V, El Kasmi F, Wünsch L, Yang Y, Fitzpatrick CR, et al. (2023). Broader functions of TIR domains in Arabidopsis immunity. Proc. Natl. Acad. Sci. USA 120, e2220921120. 10.1073/pnas.2220921120. [PubMed: 36893276]
60. Garcia-Ruiz H, Szurek B, and Van den Ackerveken G (2021). Stop helping pathogens: engineering plant susceptibility genes for durable resistance. Curr. Opin. Biotechnol. 70, 187–195. 10.1016/j.copbio.2021.05.005. [PubMed: 34153774]
61. Grant M, Brown I, Adams S, Knight M, Ainslie A, and Mansfield J (2000). The RPM1 plant disease resistance gene facilitates a rapid and sustained increase in cytosolic calcium that is necessary for the oxidative burst and hypersensitive cell death. Plant J. 23, 441–450. 10.1046/j.1365-313x.2000.00804.x. [PubMed: 10972870]
62. Henry E, Toruño TY, Jauneau A, Deslandes L, and Coaker G (2017). Direct and indirect visualization of bacterial effector delivery into diverse plant cell types during infection. Plant Cell 29, 1555–1570. 10.1105/tpc.17.00027. [PubMed: 28600390]
63. Nobori T, Velásquez AC, Wu J, Kvitko BH, Kremer JM, Wang Y, He SY, and Tsuda K (2018). Transcriptome landscape of a bacterial pathogen under plant immunity. Proc. Natl. Acad. Sci. USA 115, E3055–E3064. 10.1073/pnas.1800529115. [PubMed: 29531038]
64. Gentzel I, Giese L, Ekanayake G, Mikhail K, Zhao W, Cocuron J-C, Alonso AP, and Mackey D (2022). Dynamic nutrient acquisition from a hydrated apoplast supports biotrophic proliferation of a bacterial pathogen of maize. Cell Host Microbe 30, 502–517.e4. 10.1016/j.chom.2022.03.017. [PubMed: 35421350]

65. Hu Y, Ding Y, Cai B, Qin X, Wu J, Yuan M, Wan S, Zhao Y, and Xin X-F (2022). Bacterial effectors manipulate plant abscisic acid signaling for creation of an aqueous apoplast. Cell Host Microbe 30, 518–529.e6. 10.1016/j.chom.2022.02.002. [PubMed: 35247331]
66. Roussin-Léveillée C, Lajeunesse G, St-Amand M, Veerapen VP, Silva-Martins G, Nomura K, Brassard S, Bolaji A, He SY, and Moffett P (2022). Evolutionarily conserved bacterial effectors hijack abscisic acid signaling to induce an aqueous environment in the apoplast. Cell Host Microbe 30, 489–501.e4. 10.1016/j.chom.2022.02.006. [PubMed: 35247330]
67. van Schie CCN, and Takken FLW (2014). Susceptibility genes 101: how to be a good host. Annu. Rev. Phytopathol 52, 551–581. 10.1146/annurev-phyto-102313-045854. [PubMed: 25001453]
68. Zaidi SSEA, Mukhtar MS, and Mansoor S (2018). Genome editing: targeting susceptibility genes for plant disease resistance. Trends Biotechnol. 36, 898–906. 10.1016/j.tibtech.2018.04.005. [PubMed: 29752192]
69. Nobori T, Oliva M, Lister R, and Ecker JR (2022). PHYTOMap: multiplexed single-cell 3D spatial gene expression analysis in plant tissue. bioRxiv. 10.1101/2022.07.28.501915.
70. Baltrus DA, Feng Q, and Kvitko BH (2022). Genome context influences evolutionary flexibility of nearly identical type III effectors in two phytopathogenic Pseudomonads. Front. Microbiol 13, 826365. 10.3389/fmicb.2022.826365. [PubMed: 35250942]
71. Liu J, Elmore JM, Fuglsang AT, Palmgren MG, Staskawicz BJ, and Coaker G (2009). RIN4 functions with plasma membrane H+-AT-Pases to regulate stomatal apertures during pathogen attack. PLoS Biol. 7, e1000139. 10.1371/journal.pbio.1000139. [PubMed: 19564897]
72. La Manno G, Soldatov R, Zeisel A, Braun E, Hochgerner H, Petukhov V, Lidschreiber K, Kastriti ME, Lönnerberg P, Furlan A, et al. (2018). RNA velocity of single cells. Nature 560, 494–498. 10.1038/s41586-018-0414-6. [PubMed: 30089906]
73. Zheng GXY, Terry JM, Belgrader P, Ryvkin P, Bent ZW, Wilson R, Ziraldo SB, Wheeler TD, McDermott GP, Zhu J, et al. (2017). Massively parallel digital transcriptional profiling of single cells. Nat. Commun. 8, 14049–14112. 10.1038/ncomms14049. [PubMed: 28091601]
74. Ishizaki K, Nishihama R, Ueda M, Inoue K, Ishida S, Nishimura Y, Shikanai T, and Kohchi T (2015). Development of Gateway binary vector series with four different selection markers for the liverwort Marchantia polymorpha. PLoS One 10, e0138876. 10.1371/journal.pone.0138876. [PubMed: 26406247]
75. Zhang X, Henriques R, Lin S-S, Niu Q-W, and Chua N-H (2006). Agrobacterium-mediated transformation of Arabidopsis thaliana using the floral dip method. Nat. Protoc 1, 641–646. 10.1038/nprot.2006.97. [PubMed: 17406292]
76. Cuppels DA (1986). Generation and characterization of Tn 5 insertion mutations in Pseudomonas syringae pv. tomato. Appl. Environ. Microbiol 51, 323–327. 10.1128/aem.51.2.323-327.1986. [PubMed: 16346988]
77. Team, R.C. (2013). R: A Language and Environment for Statistical Computing.
78. Team, R. (2015). RStudio (Boston, MA: integrated development for R. RStudio, Inc.), p. 84. URL. http://www.rstudio.com 42.
79. Hao Y, Hao S, Andersen-Nissen E, Mauck WM III, Zheng S, Butler A, Lee MJ, Wilk AJ, Darby C, Zager M, et al. (2021). Integrated analysis of multimodal single-cell data. Cell 184, 3573–3587.e29. 10.1016/j.cell.2021.04.048. [PubMed: 34062119]
80. McCarthy DJ, Chen Y, and Smyth GK (2012). Differential expression analysis of multifactor RNA-Seq experiments with respect to biological variation. Nucleic Acids Res. 40, 4288–4297. 10.1093/nar/gks042. [PubMed: 22287627]
81. Robinson MD, McCarthy DJ, and Smyth GK (2010). edgeR: a Bioconductor package for differential expression analysis of digital gene expression data. Bioinformatics 26,139–140. 10.1093/bio-informatics/btp616. [PubMed: 19910308]
82. Love MI, Huber W, and Anders S (2014). Moderated estimation of fold change and dispersion for RNA-seq data with DESeq2. Genome Biol. 15, 550–621. 10.1186/s13059-014-0550-8. [PubMed: 25516281]
83. Alexa ARJ (2021). topGO: Enrichment Analysis for GeneOntology. R Package Version 2.44. 0.

84. Coppinger P, Repetti PP, Day B, Dahlbeck D, Mehlert A, and Stas-kawicz BJ (2004). Overexpression of the plasma membrane-localized NDR1 protein results in enhanced bacterial disease resistance in Arabidopsis thaliana. Plant J. 40, 225–237. [PubMed: 15447649]

Highlights

- The plant response to bacterial infection is profiled at single-cell resolution
- In a susceptible interaction, leaves contain cell populations at opposing states
- Immune markers exhibit diverse spatial and temporal expression patterns
- Susceptible markers exhibit general and sustained expression patterns

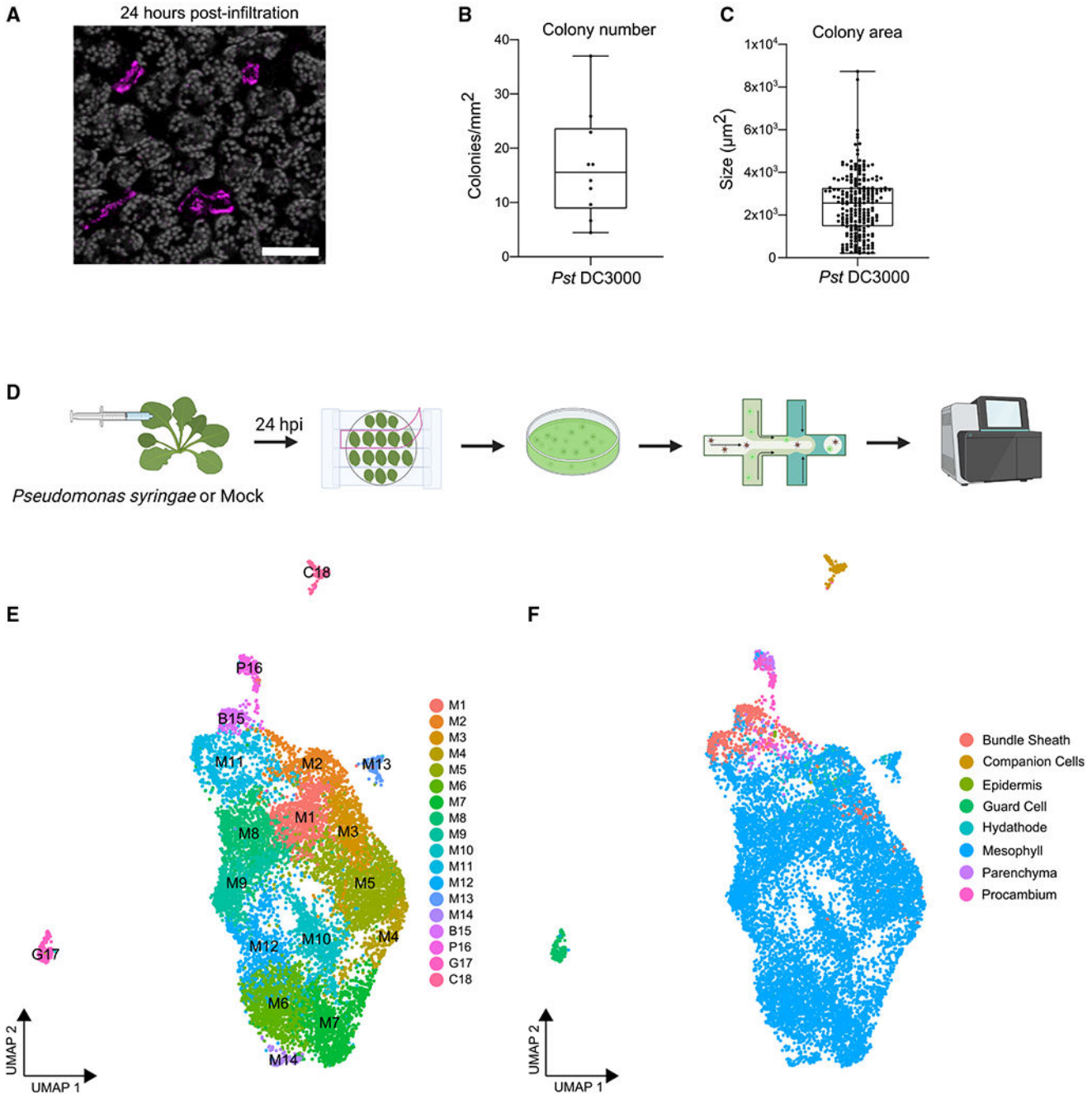

Figure 1. Single-cell RNA-seq profiling of *Arabidopsis* infected with *Pseudomonas syringae*

(A) Confocal micrograph of a representative image of an *Arabidopsis* leaf 24 h post-infiltration (hpi) with mCherry-tagged *Pst* DC3000 Δ*hopQ1* (*Pst* DC3000). The image is a maximum projection from 21 confocal z stacks. Chlorophyll autofluorescence is shown in gray. Scale bar: 100 µm.

(B and C) *Pst* DC3000 colony number and area in infiltrated leaf tissue shown in (A). Boxplot shows median with minimum and maximum values indicated (n = 10 images from 4 plants).

(D) Overview of the scRNA-seq experiment. Four-week-old *Arabidopsis* Col-0 was infiltrated with *Pst* DC3000 or 10 mM $MgCl_2$. Twenty-four hours post-infiltration, protoplasts were prepared using the Tape-*Arabidopsis* Sandwich method. Cells were isolated on the 10X Genomics Chromium chip and sequenced using the Illumina NovaSeq6000 platform.

(E and F) Single-cell uniform manifold approximation and projection (UMAP) plots from both *Pst* DC3000 and mock-treated samples, colored according to cluster identities (E) and cell types (F). M, mesophyll; B, bundle sheath; P, parenchyma and procambium; G, guard cells; C, companion cells.

See also Figures S1 and S2 and Tables S1A and S2.

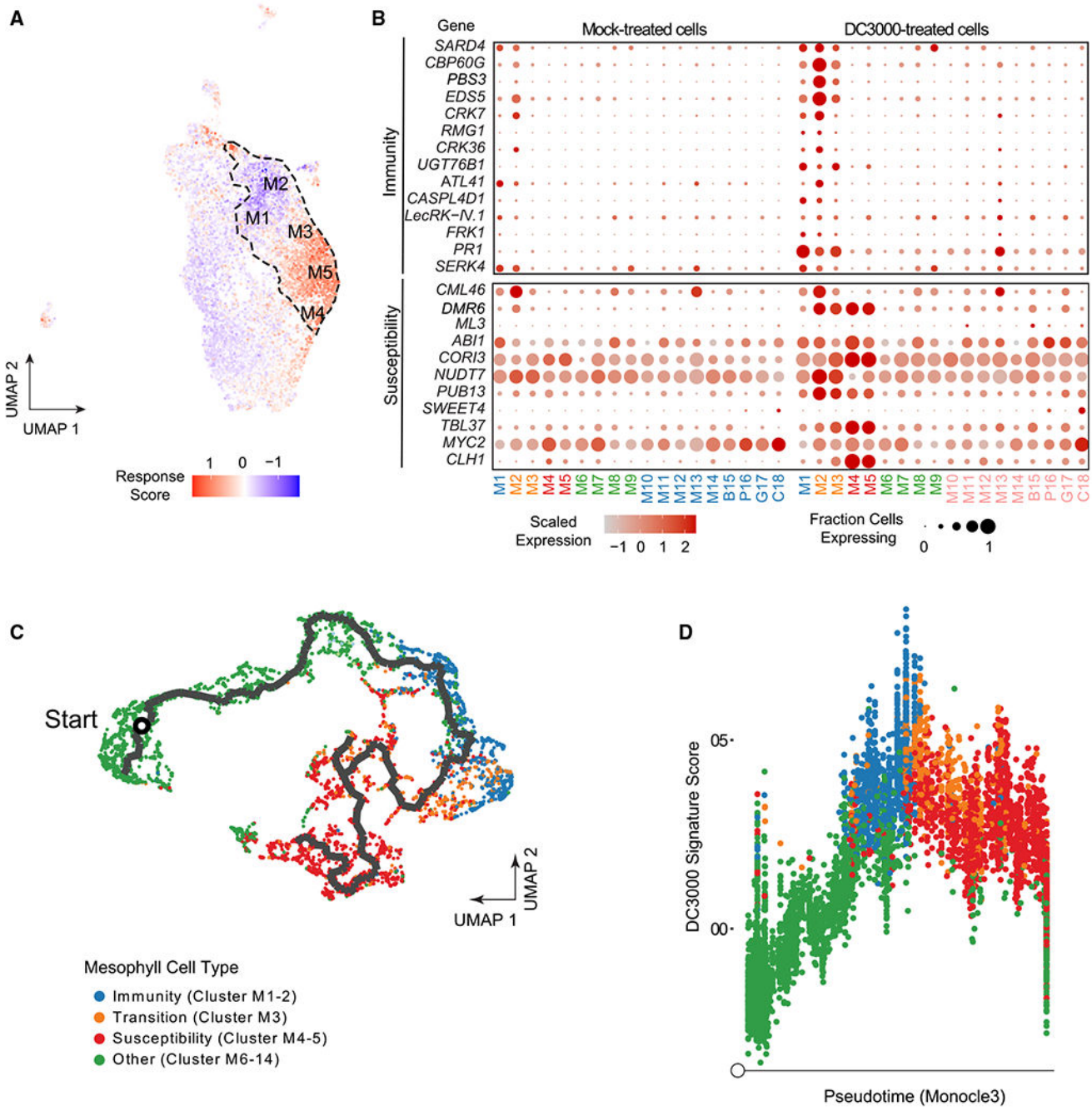

Figure 2. scRNA-seq reveals a continuum of disease progression from immune to susceptible responses within leaf tissue

(A) UMAP plot visualizing the magnitude of response to pathogen infection. Dashed line outlines the pathogen-responsive clusters (M1–M5). Immune and susceptibility response scores were calculated as gene expression modules (STAR Methods) on the basis of the cell-specific expression of sets of genes known to be involved in immunity or susceptibility that were differentially expressed in our bulk RNA-seq analysis. Blue (negative values) indicates more immune-like, red (positive values) indicates more susceptible-like.

(B) Dot plot of the relative expression and percent of cells expressing known plant immunity or susceptibility genes across different cell populations in the integrated scRNA-seq data at 24 hpi with *Pst* DC3000.

(C) Pseudotime trajectory through mesophyll cells shows directed transition from immunity (M1 and M2) to susceptibility (M4 and M5). Mesophyll cells in clusters M1–M14 were re-embedded in low-dimensional space, then subjected to trajectory inference using the Monocle 3 package (STAR Methods). An initial cell was chosen as having the lowest DC3000-induced expression signature. Cells colored by their cluster membership, with green cells belonging to non-responsive mesophyll cells (other), blue cells belonging to immune clusters, orange cells corresponding to the transition cluster, and red cells belonging to susceptibility clusters.

(D) DC3000 induction signature throughout pseudotime. Pseudotime values computed from the trajectory shown in (C). A DC3000 signature score was defined as the module score (STAR Methods) for genes repressed by DC3000 from our bulk RNA-seq analysis, subtracted from the module scores for those genes that were induced. Cells are colored as in (C), on the basis of their cluster membership.

See also Figures S2–S5 and Table S1.

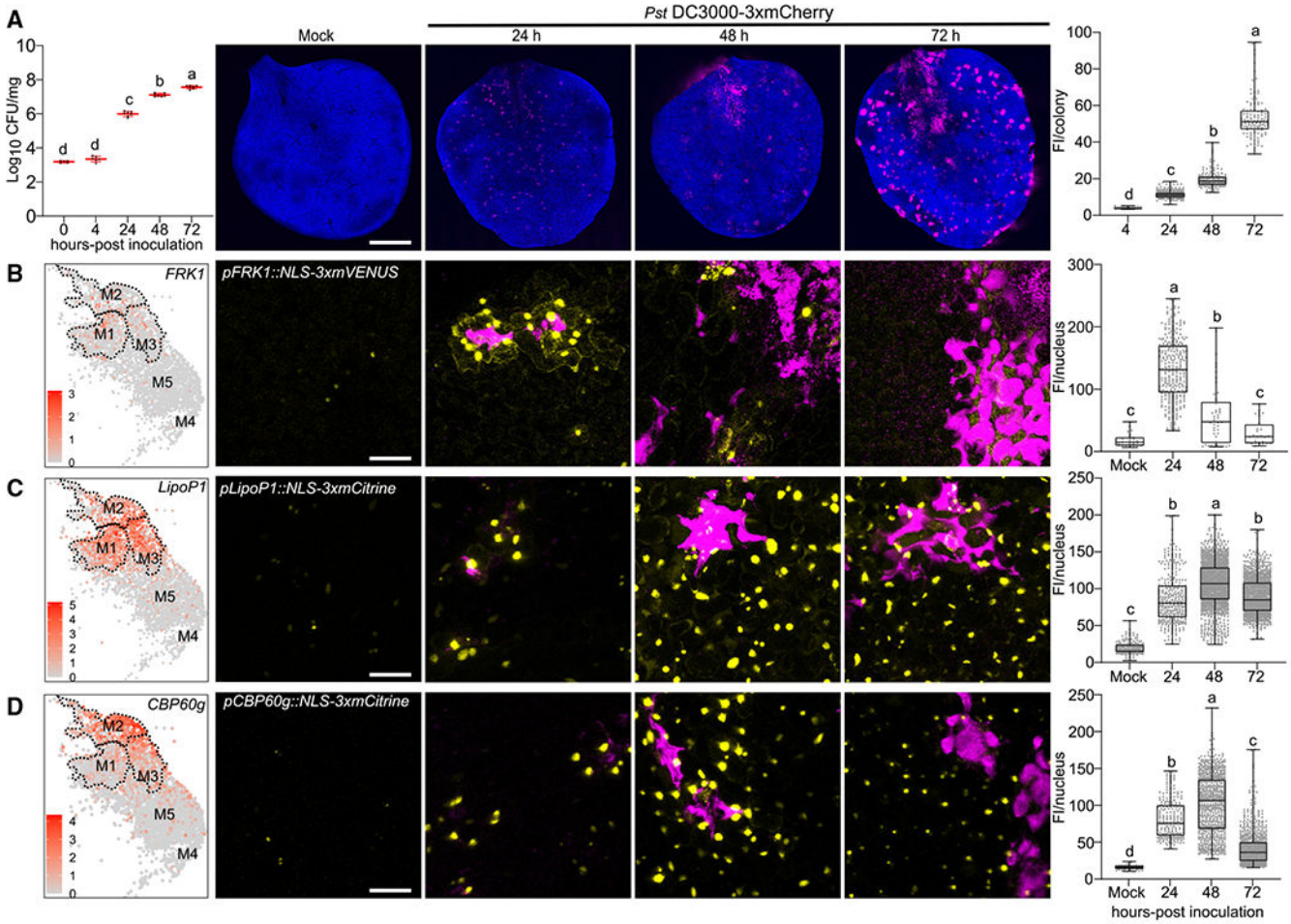

Figure 3. Temporal dynamics of immune marker expression during *Pseudomonas* infection

(A) Analysis of bacterial growth over three days post-flood inoculation. Two-week-old *Arabidopsis* seedlings grown on Murashige-Skoog plates were surfaceinoculated with mCherry-tagged *Pst* DC3000 at concentration of 1×10^7 colony-forming units/mL (CFU/mL). Left: analyses of bacterial growth over time. Middle: confocal micrograph of representative images of mock or *Pst* DC3000-inoculated *Arabidopsis* leaves over time. Chlorophyll autofluorescence is shown in blue. Right: bacterial populations were determined by quantifying mean fluorescence intensity (FI; mean gray values) per colony. Boxplots show median with minimum and maximum values (n = 3 images from 3 plants). Different letters indicate statistically significant differences ($p < 0.0001$, ANOVA with Tukey test). Scale bars: 1 mm.

(B–D) The immune markers *FRK1* (B), *LipoP1* (C), and *CBP60g* (D) are highly expressed at early infection stages but downregulated at late stages. Promoterreporter lines for each immune marker were generated by fusion to a 3xfluorophore possessing a nuclear localization signal (NLS). Left: feature plot of immune markers in pathogen-responsive clusters. Dashed line outlines clusters M1–M3. Middle: representative images of immune marker expression at different infection stages. Plants were inoculated as described in (A) and mock images are taken at 24 h. Pictures are maximum projections from confocal z

stacks. Right: mean florescence intensity per nucleus was calculated and boxplot shows median with minimum and maximum values (n = 6 images from 3 plants). Different letters indicate statistically significant differences ($p < 0.0001$, ANOVA with Tukey test). Scale bars: 25 μm. All experiments were repeated at least two times with similar results.
See also Figure S6.

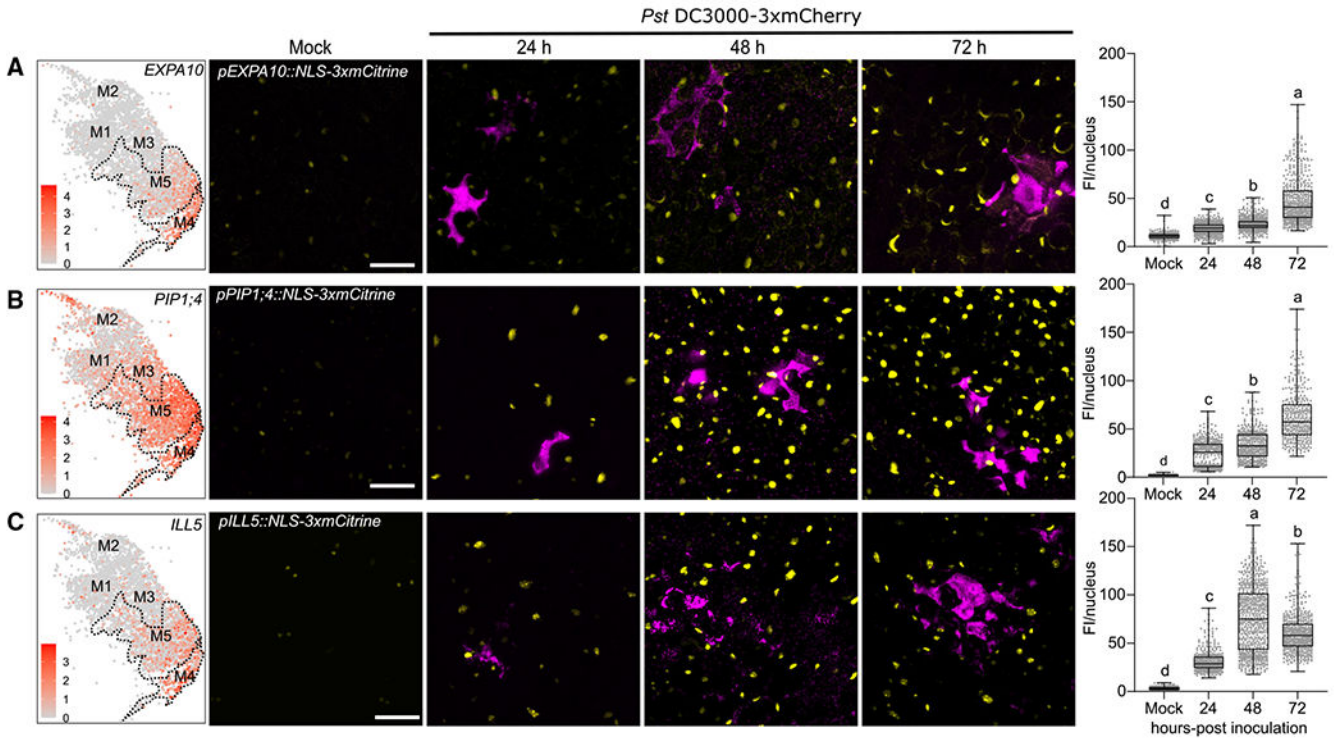

Figure 4. Temporal dynamics of susceptible marker expression during *Pseudomonas* infection

(A–C) The susceptible markers *EXPA10* (A), *PIP1;4* (B), and *ILL5* (C) are highly induced at late infection stages. Promoter-reporter lines for each marker were generated by fusion to a 3xfluorophore possessing a nuclear localization signal (NLS). Left: feature plot of susceptible markers in pathogen-responsive clusters. Dashed line outlines clusters M4 and M5. Middle: representative images of susceptible marker expression at different infection stages. Two-week-old *Arabidopsis* seedlings grown on Murashige-Skoog plates were surface-inoculated with mCherry-tagged *Pst* DC3000, and mock images were taken at 24 h. Pictures are maximum projections from confocal z stacks. Right: mean florescence intensity (FI; mean gray values) per nucleus was calculated and boxplot shows median with minimum and maximum values indicated (n = 6 images from 3 plants). Different letters indicate statistically significant differences ($p < 0.0001$, ANOVA with Tukey test). All experiments were repeated at least two times with similar results. Scale bars: 25 μm.
See also Figure S6.

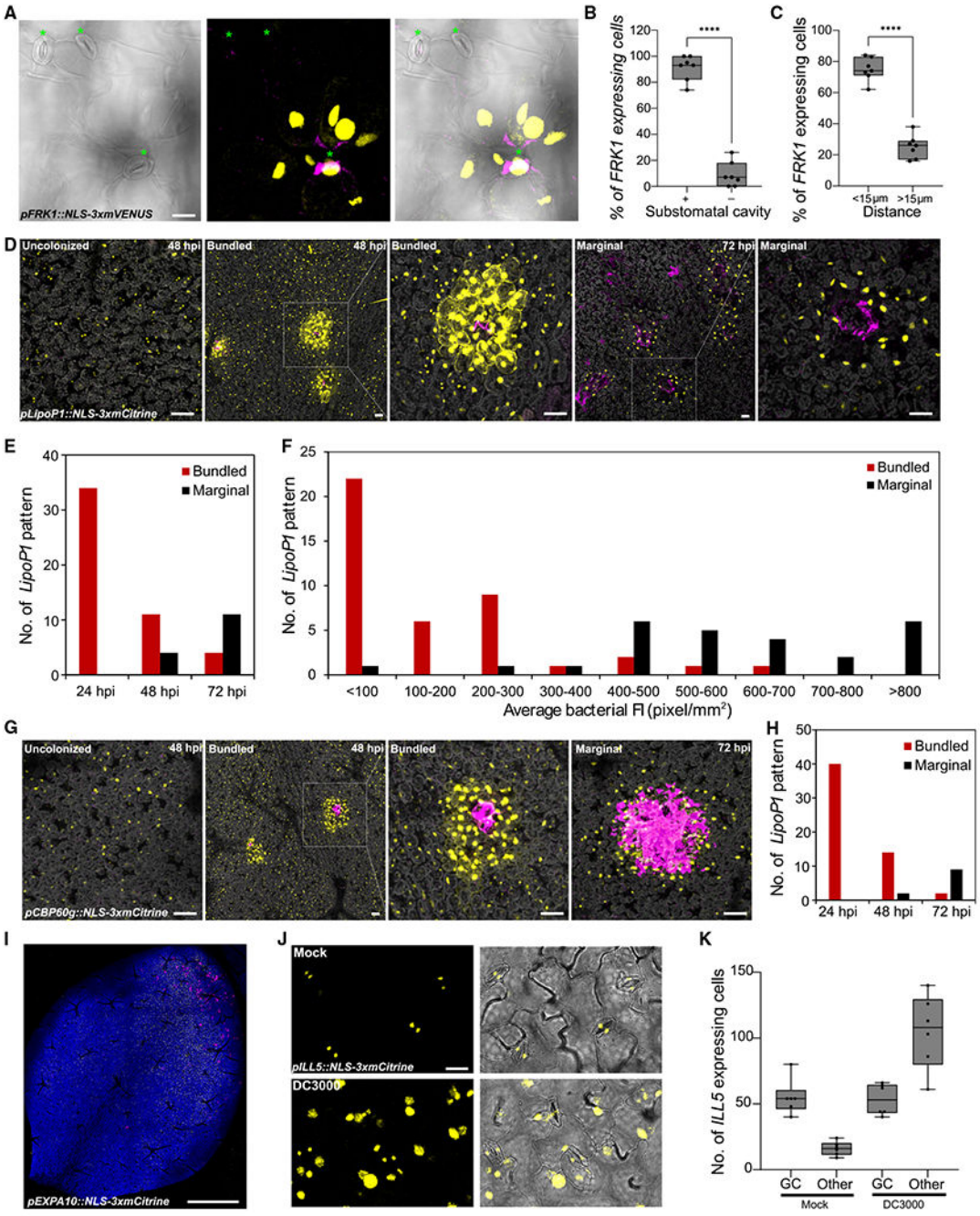

Figure 5. Spatial dynamics of immune and susceptible marker expression after *Pseudomonas* infection

(A–C) The immune marker *FRK1* is induced in surrounding cells of substomatal cavities colonized by *Pseudomonas syringae* DC3000. Two-week old *Arabidopsis pFRK1::NLS-3xmVENUS* seedlings were flood-inoculated with mCherry-tagged *Pst* DC3000. (A) At 24 hpi, whole seedlings were fixed and cleared using ClearSee. Green asterisks indicate stomata. Left: a single image of bright field channel. Middle: maximum projections of z stack of mVENUS and mCherry signals. Each yellow dot indicates a single nucleus. Right: merged image. Scale bar: 20 μm. (B) Percentage of *FRK1* expressing cells

surrounding a substomatal cavity (+) or not (−) at 24 hpi. Boxplot shows median with minimum and maximum values indicated (n = 7 images from 4 plants). ****p < 0.0001 by two-tailed, unpaired Student's t test. (C) Percentage of *FRK1* expressing cells that are proximal (<15 μm) or distal (>15 μm) to a bacterial colony 24 hpi. Data were analyzed as described in (B).

(D) The immune marker *LipoP1* is expressed in bundled and marginal patterns surrounding bacterial colonies. *Arabidopsis pLipoP1::NLS-3xmCitrine* seedlings were inoculated as described in (A). Representative images of *LipoP1* expression at 48 and 72 h in DC3000-treated samples. Pictures are maximum projections of a z stack of mCitrine, mCherry, and chlorophyll autofluorescence signals. Chlorophyll autofluorescence is shown in gray. Scale bars: 50 μm.

(E) Number of *LipoP1*-expressing patterns at 24, 48, and 72 h in DC3000-treated samples. At least 8 images from 3 plants were analyzed at each time point.

(F) Number of *LipoP1*-expressing patterns at different average florescence intensities (FIs) of bacterial colonies. Twenty-four images taken at 48 and 72 hpi were analyzed.

(G) The immune marker *CBP60g* is expressed in bundled and marginal patterns during late infection. *Arabidopsis pCBP60g::NLS-3xmCitrine* seedlings were inoculated as described in (A). Representative images of *CBP60g* expression at 48 and 72 hpi. Pictures are maximum projections of a z stack of mCitrine, mCherry, and chlorophyll autofluorescence signals. Chlorophyll autofluorescence is shown in gray. Scale bars: 50 μm.

(H) Number of *CBP60g* expressing patterns at 24, 48, and 72 hpi. At least 7 images from 3 plants were analyzed at each time point.

(I) Expression of the susceptible marker *EXPA10* in a larger area of the leaf proximal to DC3000 colonies at 24 hpi. Maximum projections of z stack of mVENUS, mCherry, and chlorophyll autofluorescence signals. Scale bars: 1 mm.

(J) The susceptible marker *ILL5* is expressed in guard cells before inoculation and broadly expressed after infection. *Arabidopsis pILL5::NLS-3xmCitrine* seedlings were inoculated as described in (A). Representative images of *ILL5* expression at 48 h in mock- or DC3000-treated samples. Maximum projections of z stack of mCitrine signals were combined with single image of bright-field channel. Scale bar: 20 μm.

(K) Number of *ILL5* expressing cells at 24 h in mock- or DC3000-treated samples. Boxplot shows median with minimum and maximum values indicated (n = 6 images from 3 plants). p < 0.0001, ANOVA with Tukey test. All experiments were repeated at least twice with similar results.

See also Figure S7, Video S1.

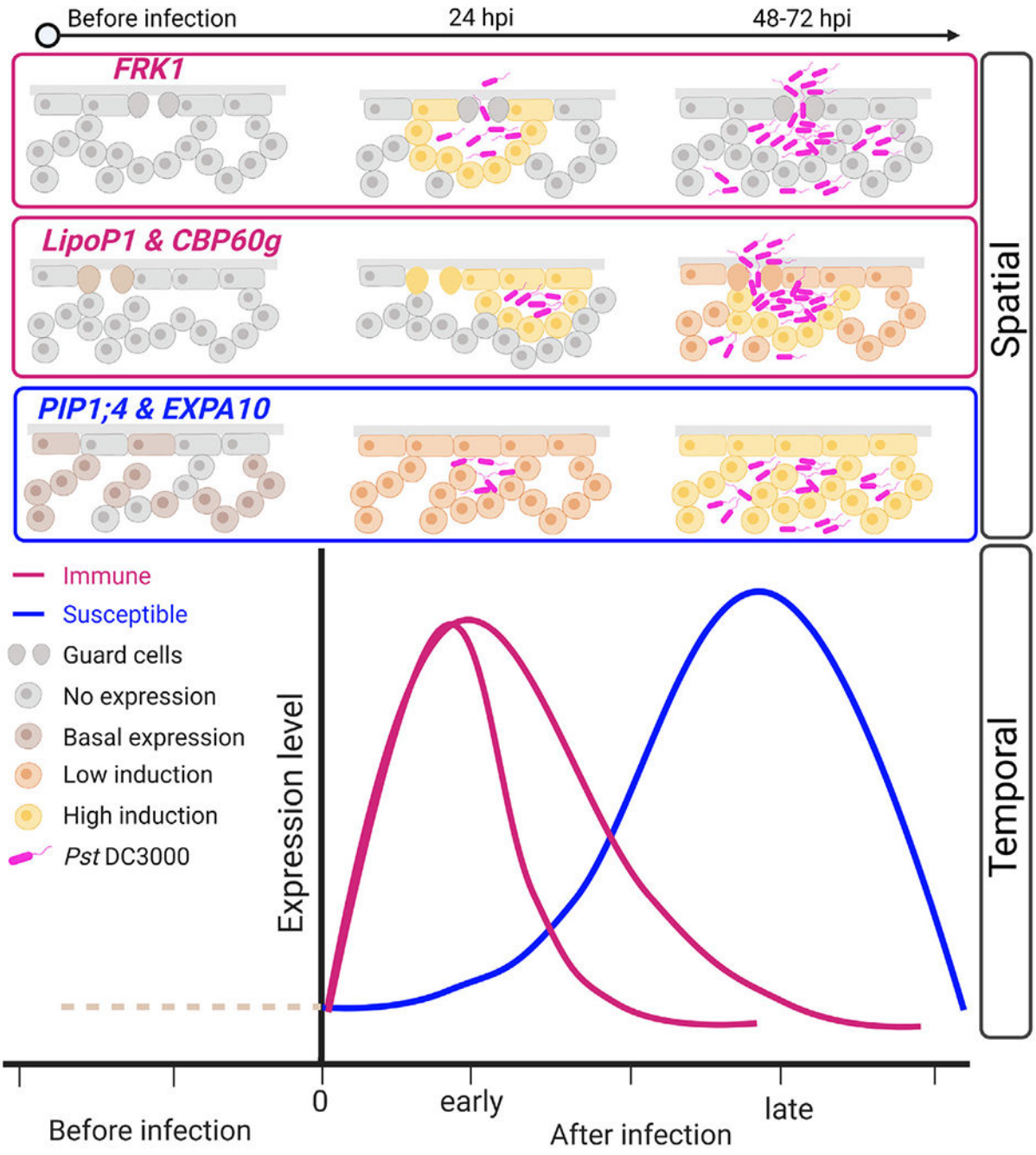

Figure 6. Spatial and temporal model of immune and susceptible marker gene expression

Immune and susceptible cell cluster markers exhibit diverse spatial and temporal expression patterns. Immune markers are highly induced at early infection stages, with in close proximity to bacterial colonies. At later time points (after 48 h), the *FRK1* marker is no longer expressed, while other immune markers, including *LipoP1* and *CBP60g*, exhibit bundled and marginal expression patterns. Susceptible cell cluster markers exhibit basal expression that is broadly induced after infection throughout the leaf and peaks at late stages.

Created with BioRender.com.

KEY RESOURCES TABLE

REAGENT or RESOURCE	SOURCE	IDENTIFIER
Bacterial and virus strains		
Pseudomonas syringae pv. tomato DC3000	Cuppels[76]	N/A
Pseudomonas syringae pv. tomato DC3000 *ΔhopQ1*	Wei et al.[28]	N/A
Pseudomonas syringae pv. tomato DC3000 *ΔhopQ1 - 3xmCherry*	This study	N/A
Pseudomonas syringae pv. tomato DC3000 - *3xmCherry*	This study	N/A
Escherichia coli strain DH5a	Fisher	Cat# 11319019
Agrobacterium tumefaciens strain GV3101	Coppinger et al.[84]	N/A
Chemicals, peptides, and recombinant proteins		
Cellulase Onuzuka R10	Yakult	Cat# L0012
Macerozyme R10	Yakult	Cat# L0021
Mannitol	Sigma	Cat# M4125-5KG
MES (2-(N-Morpholino)ethanesulfonic acid hydrate)	Fisher	Cat# BP300-100
Bovine Serum Albumin (BSA)	Fisher	Cat# BP1600-100
Sucrose	Fisher	Cat# BP220-212
Tween-20	Fisher	Cat# BP337-500
Silwet-77	Bioworld (Fisher)	Cat# NC0138454
β-mercaptoethanol	Amersco (VWR)	Cat# M131-100ML
KCl	Mallinckrodt	Cat# 6858
MS medium	RPI (Fisher)	Cat# 50-213-423
Trizol	Invitrogen (Fisher)	Cat# 15596018
Dulbecco's Phosphate-buffered saline (DPBS, 1X)	Cellgro	Cat# 21-031-CV
Xylitol	Fisher	Cat# AAA1694422
Sodium deoxycholate	Sigma	Cat# D6750-500G
Urea	Fisher	Cat# U15-3
Paraformaldehyde	Sigma	Cat# P6148
Rifampicin	Fisher	Cat# BP2679-5
Spectinomycin	Sigma	Cat# 56757010GM
Hygromycin	Gibco (Fisher)	Cat# 10687010
Carbenicillin	Fisher	Cat# BP2648-5
$MgCl_2$	Fisher	Cat# M35-212
Sodium Hydroxide	Fisher	Cat# S230-500
Critical commercial assays		
In-Fusion HD Cloning Plus	Clontech/Takara	Cat# 638910
pENTR Directional TOPO Cloning kit	Invitrogen	Cat# K2400-20

REAGENT or RESOURCE	SOURCE	IDENTIFIER
Gateway Cloning Technology LR	Invitrogen	Cat# 11791-020
RQ1 RNase-Free DNase	Promega	Cat# M6101
Chromium Single Cell 3' reagent kit V3	10X Genomics	Cat# PN-1000268
QuantSeq FWD kit	Lexogen	Cat# 015
Kapa Library Quantification kit	Kapa Biosystems/Roche	Cat# 07960484001
Deposited data		
scRNA-seq and bulk RNA-seq datasets	This study	GSE213625
Original microscopy images	This study	https://doi.org/10.5281/zenodo.7686553
Original code	This study	https://doi.org/10.5281/zenodo.7888124
Experimental models: Organisms/strains		
Arabidopsis thaliana: Col-0 wild-type	ABRC (*Arabidopsis* Biological Resource Center)	CS70000
Arabidopsis: pFRK1::NLS-3xmVENUS	Zhou et al.[46]	N/A
Arabidopsis: pLipop1::NLS-3xmCitrine (Line 1, 19-10-5)	This study	ABRC: CS73265
Arabidopsis: pLipop1::NLS-3xmCitrine (Line 2, 19-15-1)	This study	ABRC: CS73266
Arabidopsis: pCBP60g::NLS-3xmCitrine (Line 1, 22-4)	This study	ABRC: CS73260
Arabidopsis: pCBP60g::NLS-3xmCitrine (Line 2, 22-1)	This study	ABRC: CS73408
Arabidopsis: pEXPA10::NLS-3xmCitrine (Line 1, 16-7-3)	This study	ABRC: CS73261
Arabidopsis: pEXPA10::NLS-3xmCitrine (Line 2, 16-8)	This study	ABRC: CS73262
Arabidopsis: pPIP1;4::NLS-3xmCitrine (Line 1, 23-4)	This study	ABRC: CS73267
Arabidopsis: pPIP1;4::NLS-3xmCitrine (Line 2, 23-5)	This study	ABRC: CS73268
Arabidopsis: pILL5::NLS-3xmCitrine (Line 1, 4-5-1)	This study	ABRC: CS73263
Arabidopsis: pILL5::NLS-3xmCitrine (Line 2, 4-1-3)	This study	ABRC: CS73264
Oligonucleotides		
All primers are listed in Table S3	This study	N/A
Recombinant DNA		
pLipop1::NLS-3xmCitrine	This study	Addgene: 192522
pCBP60g::NLS-3xmCitrine	This study	Addgene: 192521
pPIP1;4::NLS-3xmCitrine	This study	Addgene: 192524
pILL5::NLS-3xmCitrine	This study	Addgene: 192525
pEXPA10::NLS-3xmCitrine	This study	Addgene: 192523
Software and algorithms		
Leica Application Suite X (v3.4.2.18368)	Leica Microsystems	https://www.leica-microsystems.com/
Zeiss Zen 2.3 SP1 FP1 (v14.0.12.201)	Zeiss	https://www.zeiss.com/corporate/int/home.html

REAGENT or RESOURCE	SOURCE	IDENTIFIER
GraphPad Prism (v9.2.0)	GraphPad	https://www.graphpad.com
Imaris (v8.0)	Oxford Instruments Imaris	https://imaris.oxinst.com/
Geneious Prime (v2021.1.1)	Geneious	www.geneious.com
R/RStudio (v1.4.1103)	R CoreTeam[77] RStudio Team[78]	https://www.r-project.org/
Seurat (v3.9.9005)	Hao et al.[79]	https://github.com/satijalab/seurat
TrimGalore	https://www.bioinformatics.babraham.ac.uk/projects/trim_galore/	https://github.com/FelixKrueger/TrimGalore
EdgeR (v3.12)	McCarthy et al.[80] Robinson et al.[81]	https://bioconductor.org/packages/release/bioc/html/edgeR.html
Cellranger (v6.0.1)	10x Genomics	https://support.10xgenomics.com/single-cell-gene-expression/software/pipelines/latest/installation
Velocyto (v0.17.15)	La Manno et al.[72]	http://velocyto.org/
Monocle 3 (v1.0.0)	Trapnell et al.[37] Qiu et al.[40]	https://github.com/cole-trapnell-lab/monocle3
DESeq2 (v1.30.1)	Love et al.[82]	https://bioconductor.org/packages/release/bioc/html/DESeq2.html
topGO (v3.12)	Alexa and Rahnenfuhrer[83]	https://bioconductor.org/packages/release/bioc/html/topGO.html